Oxidation of Ethylene-Air Mixtures at Elevated Pressures, Part 2: Chemical Kinetics

Madeleine M. Kopp[1] and Eric L. Petersen[2]
Texas A&M University, College Station, Texas, 77843

and

Wayne K. Metcalfe[3], Sinéad M. Burke[4], and Henry J. Curran[5]
National University of Ireland, Galway, Ireland

A chemical kinetics sub-mechanism for small molecular weight hydrocarbons was modified by adjusting rate constants in order to produce better agreement with recent ethylene ignition delay time data compared to an earlier version of the mechanism, for temperatures from 1003 to 1401 K, at pressures between 1.1 and 24.9 atm and for equivalence ratios from 0.3 to 2.0. The improved mechanism captures the pressure and equivalence ratio behavior seen in the data at these intermediate temperatures, such as the smaller-than-expected effect of equivalence ratio at the higher temperatures and an apparent lack of pressure dependence at lean conditions. By using detailed sensitivity analyses, the important reactions were identified, rectifying the model simulations in predicting the observed experimental behavior of the data in this study. In fact, when the model is used to extend the temperature range above 1400 K and below 1000 K, the same pressure dependence is actually seen for all equivalence ratios, just to a lesser extent at the test temperatures. Hence, the resulting hydrocarbon mechanism is much more robust as a result of this exercise. The initial deficiency and subsequent improvement of the model justifies the new ignition data from Part 1 as well as the need for further study on ethylene kinetics.

Deleted: lower-order

Deleted: than what was seen in

Deleted: namely

Deleted: ;

Deleted: ;

Deleted: -

Deleted: of

[1] Research Assistant, Department of Mechanical Engineering, 3123 TAMU.
[2] Professor, Department of Mechanical Engineering, 3123 TAMU, Senior Member AIAA.
[3] Postdoctoral Researcher, Combustion Chemistry Centre.
[4] Postgraduate Student, Combustion Chemistry Centre.
[5] Director, Combustion Chemistry Centre.

I. Introduction

Despite the importance of ethylene as an intermediate species in the combustion and oxidation of large molecular weight hydrocarbons, surprisingly few data exist for the ignition of C_2H_4 at fuel-air concentrations and at elevated pressures and temperatures. Presented in the paper by Kopp et al. [1], new ignition delay time experiments were obtained for pressures ranging from 1 to 25 atm over a range of C_2H_4-air equivalence ratios from 0.3 to 2.0. These data were measured in a shock tube behind reflected shock waves over a temperature range of about 1000–1400 K. As shown in Kopp et al. [1], the ignition delay time data exhibited some arguably unexpected trends with pressure (p) and equivalence ratio (ϕ). At all pressures, a very small effect of equivalence ratio on ignition delay times was observed experimentally at higher temperatures. Another tendency of the experimental results was that at lean equivalence ratios, there was no pressure dependence in the ignition delay times within the uncertainty of the measurements. On the other hand, for $\phi = 1$ and 2, pressure had a more apparent impact on the chemical reactivity, with higher pressures leading to shorter ignition delay times, as expected.

Also shown in Kopp et al. [1] were the results of an improved chemical kinetics model. These improvements were required because the authors' C_1–C_4 chemical kinetics mechanism at the time of the original data set was unable to satisfactorily predict both the absolute level of ignition delay time and its trends with pressure and ϕ. The purpose of Part 2 of the study was to provide the details on the changes made to the chemical kinetics model and, more importantly, to provide insights into the unusual chemical kinetic behavior seen in the ethylene ignition delay time data. The present paper begins discussing the chemical kinetics modeling immediately following the introduction; background information on ethylene ignition delay time data from the literature can be found in Kopp et al. [1]. Initially, details of the chemical kinetic steps that were modified are provided. The first trends to be investigated are the effects of equivalence ratio at constant pressures, and ignition sensitivity and species flux analyses are provided to highlight the dominant reactions driving C_2H_4 ignition behavior. Thereafter, the trends of pressure at constant ϕ a□□□□□□□□□□□□. In the latter portion of the paper, the model is compared to other data from the literature, primarily those obtained under highly diluted conditions. The current model is then compared to some other modern, detailed mechanisms.

Deleted: higher-order

Deleted: real

Deleted: near 1 atm

Deleted: there appeared to be

Deleted: little

Deleted: the

Deleted: ; this effect lessened somewhat at higher pressures

Deleted: interesting

Deleted: D

Deleted: n

Deleted: at the start

Deleted: the

Deleted: Discussed next are

Deleted: .

Deleted: r

II. Chemical Kinetic Model and Calculations

As mentioned above, an improved chemical kinetics model was compiled using ethylene data as the primary target. All simulations were performed using the aurora module in the CHEMKIN-PRO package [2]. Constant internal energy and constant volume were assumed in the calculations to match the shock-tube experiments, which showed no pre-ignition pressure rise, but which exhibited significant pressure increases during the ignition event for all mixtures. The mixtures studied are provided in Kopp et al. [1] but are summarized briefly here. Four equivalence ratios were tested (0.3, 0.5, 1.0, and 2.0) for $C_2H_4/O_2/N_2$ mixtures with the ratio between N_2 and O_2 being 3.76 by volume to mimic ideal air.

The foundation of the detailed kinetics mechanism is the H_2/O_2 sub-mechanism of Ó Conaire *et al.* [3], together with the C_2, C_3, and CO/CH_4 sub-mechanisms published previously [4–6]. Three recent papers on the butane isomers detail the C_4 sub-mechanism [7–9] and CH_4-based blends [10,11]. Presented in the following paragraphs are the changes that were made to the original mechanism to produce the current version of the model. Table 1 includes the main reactions of the improved ethylene sub-mechanism. The complete mechanism, thermodynamics, and transport properties can be found in the supplemental material to the present paper. The version of the updated mechanism developed here, AramcoMech 1.3 [12], is based on the C4_49 version. A brief summary of the changes is described below, with only the alterations pertinent to the current study discussed in detail. The thermodynamic properties have been updated to recent values [13], where available.

As mentioned above, the H_2/CO sub mechanism is based on the work of Ó Conaire *et al.* [3] with the most recent updates described in Kéromnès *et al.* [14,15]. Recent changes to the C_1–C_3 mechanism can be found in Lowry *et al.* [16], Metcalfe *et al.* [12] and Aul *et al.* [17]. The chemistry of some important unsaturated species including 1,3-butadiene, propene, and allene have also been updated, adopting the work of Laskin *et al.* [18], which is primarily based on the earlier studies of Davis *et al.* [19].

Deleted: the e

Deleted: 2

Deleted: 3

Deleted: 4

Deleted: 5

Deleted: 6

A. $C_2H_4(+M) \rightleftarrows H_2CC+H_2(+M)$

The rate constant for this reaction has been adopted from GRI 3.0 [20], but following the recommendations of Wang *et al.* [21], the products have been altered to include vinylidene instead of acetylene. However, this reaction proved unimportant at the conditions investigated in this study due to its high activation energy.

B. $C_2H_4+\dot{O}\dot{O} \rightleftarrows CH_2CH\dot{O}\dot{O}+\dot{H}$ / $\dot{C}H_3+H\dot{C}O$

The branching ratio of this reaction was found to be critical to match the experimentally observed, low-pressure (1.1 atm) reactivity, especially under fuel-lean conditions. The original mechanism utilized the recommendation of Baulch *et al.* [22] which afforded a branching ratio of approximately 60:35 in favor of methyl and formyl radical formation. A third channel producing CH_2CO (ketene) + H_2 was ascribed a 5% weighting. A recent theoretical study from Nguyen *et al.* [23] produced a total rate constant similar to Baulch *et al.*'s recommendation but with different product ratios. The theoretical study predicts the same major products as Baulch *et al.*, but the formation of formaldehyde and triplet methylene also becomes an important product set as the temperature increases. The study also predicts three other minor product channels, accounting for approximately ten percent of the total rate constant. Both the total rate constants and the branching ratios arising from both descriptions are presented in Fig. 1.

It was not possible to reconcile the current kinetic scheme using either reaction description to the experimental data observed in Part 1 of this study [1]. To improve the performance of the model, the recommended product distribution of Baulch *et al.* was modified slightly from a 60:35 to a 55:45 ($\dot{C}H_3+H\dot{C}O$: $CH_2CH\dot{O}\dot{O}+\dot{H}$) branching ratio, with the channel forming $CH_2CO + H_2$ not included, while retaining the same total rate constant. This change is within the uncertainty of 10% in the temperature range 300 – 1000 K rising to 30% at temperatures below and

Deleted: the
Deleted: to reaction
Deleted: CH_2CH
Deleted: predicted
Deleted: 40
Formatted: Subscript
Formatted: Subscript
Deleted: ation
Deleted: CH_2CH
Formatted: Not Superscript/ Subscript

above this as given by Baulch *et al.* The small shift towards the ketene and atomic oxygen product set improved model agreement significantly at low-pressure, hydrogen-atom-lean conditions. The importance of this reaction is highlighted again in the discussion section.

C. $C_2H_4 + \dot{O}H \rightleftarrows \dot{C}_2H_3 + H_2O$

The rate constant for this reaction has been adopted from the recent measurements of Vasu *et al.* [24]. The hydroxyl radical can undergo a more complex interaction with ethylene involving addition and subsequent decomposition to a variety of product sets, Table 1. The rate constants for these reactions, including the formation of formaldehyde, acetaldehyde, and vinyl alcohol were taken from a detailed theoretical study by Senosiain *et al.* [25]. In that study, theoretical values for the direct abstraction reaction were also provided. At temperatures in the range 1000 – 2000 K, this value is approximately 30% lower than the experimentally determined value of Vasu *et al.* The experimental value was chosen as it improves agreement with the ignition delay time data in the present study and with lean laminar flame speed measurements. Additional validation targets, including laminar burning velocities, are provided later in this paper.

D. $C_2H_4 + H\dot{O}_2 \rightleftarrows C_2H_4O1\text{-}2 + \dot{O}H$

The addition of a hydroperoxyl radical to ethylene to form oxirane and a reactive hydroxyl radical is an important reaction at low-temperature (< 1000 K), high-pressure (> 10 atm) conditions, particularly at fuel-rich conditions, Fig. 6(a). To improve model agreement for the ethylene mixtures, it was necessary to reduce the original recommendation from Baulch *et al.* [26] by a factor of four.

Formatted: Font: Italic

Deleted: percent

Deleted:

E. $\dot{C}_2H_3+O_2 \rightleftarrows CH_2CH\dot{O} + \dot{O}\dot{O} / CH_2O+H\dot{C}O / CH_2O+CO+\dot{H}$

The vinyl plus molecular oxygen system is of critical importance to ethylene oxidation. It also plays a significant role in the reactivity of larger hydrocarbon fuels as ethylene can be formed in significant concentrations via hydrogen abstraction followed by β-scission. Despite several studies [27–30], there remains significant uncertainty in the understanding of this reaction, and in particular the temperature where the dominant product set switches from chain propagation, (CH_2O + $H\dot{C}O$) to chain branching ($CH_2CH\dot{O}$ + $\dot{O}\dot{O}$). The description from Marinov *et al.* [31] has been adopted in this work as it results in good agreement over a wide variety of conditions and experimental setups, including speciation data from flow- and jet-stirred reactors and laminar flame measurements. The minor channel in the Marinov *et al.* description forming acetylene and hydroperoxyl radical was replaced by the formation of formaldehyde, carbon monoxide, and a hydrogen atom—a product set predicted by Klippenstein *et al.* [29]. This alteration improved the model prediction of acetylene species concentration profiles from the jet-stirred reactor study of Dagaut *et al.* [32].

Deleted:

Deleted: ¶

F. $CH_2CH\dot{O}(+M) \rightleftarrows CH_2CO+\dot{H}/\dot{C}H_3+CO(+M)$

Rate constants describing vinoxy radical decomposition were adopted from a recent theoretical study by Senosiain *et al.* [33]. Rate constant expressions provided at individual pressures were used to generate pressure-dependent expressions in the Troe format [34]. Once again, in an attempt to improve agreement at the lower pressures of this study, the resulting low-pressure limit for ketene plus $\dot{H}$-atom production was increased by a factor of two, thus making this channel more competitive at lower pressures, resulting in an overall increase in reactivity.

III. Results and Discussion

A summary of experiments that were performed under the present study is discussed in more detail in Kopp et al. [1]. The following figures represent experimental results plotted on Arrhenius-type plots that give the ignition delay time, τ_{ign}, on a log scale as a function of the reciprocal reflected-shock temperature. The results of the improved chemical kinetics mechanism are also shown in each of the plots in comparison with the data. In general, the agreement between model and data is favorable yet greatly improved over the original version of the model. Note that in the comparisons between model and data presented below and originally elsewhere [1], the unusual behavior of ethylene ignition kinetics compared to other hydrocarbons is emphasized by providing two temperature scales within each plot. The original, zoomed-in version is provided as an inset to the main plot which shows a much wider temperature range. We found that such a plot is critical to describing and understanding the C_2H_4 ignition kinetics, as is elaborated upon in the following sections.

Deleted: idiosyncrasies

Deleted: the

Deleted: are

A. Equivalence Ratio Dependence

Figures 2–4 depict the effect of equivalence ratio, with the simulations plotted over an exaggerated temperature scale to highlight the unusual temperature dependence that is not evident from the temperature range of the experimental study. Figure 2 shows the experimental data and simulations at low pressure as a function of equivalence ratio. On the large scale of the outer figure, the experimental data appear to show very little effect of

fuel oxygen ratio. Over the temperature range of the experimental study however, a small, yet noticeable equivalence ratio dependence is evident, with the reactivity increasing when moving from fuel-rich to fuel-lean conditions. This effect of equivalence ratio is typical of high-temperature hydrocarbon oxidation, where the chain branching reaction between hydrogen atom and molecular oxygen to produce an oxygen atom and a hydroxyl radical dominates reactivity. Fuel molecules compete with molecular oxygen for hydrogen atoms, preventing chain branching. Thus, an increased fuel concentration inhibits reactivity.

The predicted equivalence ratio dependence is significantly more interesting when viewed over a wider temperature scale, where it mimics a typical alkane until the highest temperatures (> 1250 K). At low temperatures, fuel-rich mixtures are more reactive as the main chain branching pathways generally emanate from the fuel species. As the temperature increases, the leaner mixtures exhibit higher reactivity due to the increased importance of the aforementioned chain branching reaction between hydrogen atoms and molecular oxygen. However, this characteristic is much less significant in ethylene than for a typical alkane [7,8]. As the temperature is increased further, this dependence disappears, with the predicted reactivity essentially the same for all equivalence ratios. This behavior is very unusual when compared to typical hydrocarbons, where fuel-lean mixtures continue to be more reactive at higher temperatures (> 1250 K) due to hydrogen/oxygen chain branching system.

The effect of equivalence ratio on ignition delay time at higher pressures shown in Figs. 3 and 4 is very similar to that found at atmospheric pressure, where there is a significant dependence at lower temperature where fuel-rich mixtures are faster and fuel-lean mixtures slower to ignite compared to stoichiometric ones. There is a minimal dependence on equivalence ratio at higher temperatures. Examining the dependence over the experimental temperature range in isolation, there is a noticeable increase in equivalence ratio dependence as the pressure increases, both in the experimental results and in the model predictions, Figs. 2–4. However, the simulations suggest that the temperature at which the reactivity of the different mixtures converges simply moves to a higher temperature as the pressure increases. It is seen in Fig. 2 that, at 1 atm and at temperatures below 1050 K, fuel-rich mixtures are predicted to be faster than fuel-lean ones. At temperatures above this, there is a change in behavior where all equivalence ratios are predicted and measured to have almost identical ignition delay times. At the higher pressure of 10.3 atm, Fig. 3, this changeover in behavior shifts to a higher temperature, closer to 1200 K. This is also reflected in Fig. 4 where the changeover temperature shifts to 1250 K at 22.7 atm.

Deleted: The model under-predicts reactivity for the leanest mixtures, but correctly matches the trend found in the data as well as the absolute values of ignition delay time.¶

Deleted:

Deleted: hydrocarbon

Deleted: essentially

Deleted:

Analogous behavior is visible in a typical alkane [7], where the temperature at which fuel-rich mixtures transition from most reactive to least reactive increases with elevated pressures. The characteristic is caused by the competition between the chain branching reaction $\dot{H}+O_2 \rightleftarrows \ddot{O}+\dot{O}H$ and the pressure-dependent, stabilization/propagation reaction $\dot{H}+O_2(+M) \rightleftarrows H\dot{O}_2(+M)$, forming the hydroperoxyl radical. At higher pressures, a higher temperature is required for the chain branching pathway to become the most significant. Therefore, the shift in hydrocarbon reactivity-controlling kinetics to the $\dot{H}/O_2$ system occurs at a higher temperature at 20 atm when compared to, for example, 1 atm.

In an attempt to explain the features of Fig. 2, brute-force sensitivity analyses were performed at atmospheric pressure and equivalence ratios of 0.3 and 2.0 as a function of temperature, as displayed in Fig. 5 for three different temperatures (1000, 1200, and 1400 K). This analysis was performed by increasing and decreasing each reaction rate expression by a factor of two and calculating the effect on the predicted ignition delay time. The sensitivity coefficient (σ) is defined as:

$$\sigma = \log\left(\tau'/\tau''\right)\Big/\log\left(2.0/0.5\right)$$

where τ' is the ignition delay time calculated with the increased rate coefficient, and τ'' is the ignition delay time calculated using the decreased rate expression. A negative sensitivity coefficient indicates an overall promoting effect, while a positive coefficient is indicative of an inhibiting effect on reactivity. Flux analyses have also been carried out at a time of 20 percent fuel consumption and are discussed where beneficial to further elucidate the underlying kinetics.

At 1000 K, where a noticeable equivalence ratio dependence is evident, Fig. 5a highlights the importance of the reaction between the vinyl radical and molecular oxygen, with the chain branching pathway producing oxygen

atoms and vinoxy radicals the most promoting, and the propagation route forming formaldehyde and formyl radicals the most inhibiting. The concentration of vinyl radicals is significantly higher in the fuel-rich case, thus explaining the higher reactivity predicted by the current kinetic scheme. The flux analysis results for selected species are presented in Table 2 and highlight the increased rate of the vinyl plus molecular oxygen reaction. Figure 5a also depicts quite significant differences in the relative sensitivities of some reactions depending on the equivalence ratio.

Deleted:

Under fuel-lean conditions, an increased importance on the reactions $\dot{H}+O_2 \rightleftarrows \dot{O}\dot{H}+\dot{O}$ H and $C_2H_4+\dot{H}$ $(+M) \rightleftarrows \dot{C}_2H_5$ $(+M)$ is evident. This result can be explained by examining the $\dot{H}$-atom flux in Table 2, which shows that under fuel-lean conditions, the above reactions are the primary $\dot{H}$ atom consumption pathways, while being much less significant under fuel-rich conditions.

As the temperature is increased, there is a significant shift in the reactivity-controlling kinetics under fuel-lean conditions, Fig. 5b. The chain branching reactions $\dot{H}+O_2 \rightleftarrows \dot{O}\dot{H}+\dot{O}$ H and $C_2H_4+\dot{O}\dot{O} \rightleftarrows CH_2CH\dot{O}+\dot{H}$ now dominate reactivity, with vinyl chemistry playing a much smaller role. The increasing importance of $\dot{H}+O_2 \rightleftarrows \dot{O}\dot{H}+\dot{O}$ H with increasing temperature is typical of hydrocarbon oxidation at high temperatures. It is also the main source of oxygen atoms which leads to the increase in sensitivity of the ethylene plus atomic oxygen reaction. At fuel-rich conditions,

Deleted:

these reactions are also of an increased importance, with $\dot{H}+O_2 \rightleftarrows \dot{O}\dot{H}+\dot{O}H$ having an almost identical sensitivity as $\dot{C}_2H_3+O_2 \rightleftarrows CH_2CH\dot{O}\dot{O}+\dot{O}\dot{O}$. The most striking result of the analysis, shown in Fig. 5b, is the promoting effect of $\dot{H}$-atom abstraction from the fuel by $\dot{H}$ atoms to form a vinyl radical plus molecular hydrogen, and helps explain the lack of equivalence ratio dependence at higher temperatures. This result is the opposite of what is observed for other hydrocarbons in the high-temperature regime, where fuel molecules consuming $\dot{H}$ atoms reduce reactivity as it prevents chain branching via $\dot{H}+O_2 \rightleftarrows \dot{O}\dot{H}+\dot{O}H$. However, in the case of ethylene, the product of the abstraction, namely the vinyl radical, also undergoes chain branching through reaction with molecular oxygen, thus no inhibition is observed. Under fuel-rich conditions, there is a marked increase in the sensitivity of hydrogen-atom abstraction from the fuel by methyl radicals when compared to the value calculated at fuel-lean conditions. This increased sensitivity to H-atom abstraction is due to the larger ethylene and subsequent methyl radical concentration formed via vinoxy radical decomposition and the reaction $C_2H_4+\dot{O}\dot{O} \rightleftarrows \dot{C}H_3+H\dot{C}O$. The promoting effect is a consequence of the formation of a vinyl radical which then contributes to chain branching by reacting with molecular oxygen.

Deleted: CH_2CH

Deleted:

Deleted: C

Deleted: H

Deleted: h

Deleted: ¶

A sensitivity analysis was also performed at 1400 K, where the model predicts essentially zero dependence on equivalence ratio. The results depicted in Fig. 5c are very similar to those obtained at 1200 K, except that the hydrogen/oxygen chain branching system dominates reactivity further for both equivalence ratios. Again, the competition between molecular oxygen and the fuel for $\dot{H}$ atoms becomes somewhat irrelevant as exponential radical growth results from both processes.

$\dot{H}\dot{H}\dot{O}\dot{H}\dot{O}\dot{H}$To illustrate the similar behavior at low and high pressure, the sensitivity analysis described in Fig. 5 was repeated at the same temperatures and equivalence ratios but at a larger pressure of 22 atm. The results are depicted in Fig. 6. The equivalence ratio dependence is more explicitly demonstrated at higher pressure. At low temperature, Fig. 6a, vinyl radical chemistry is completely dominant at both equivalence ratios with minor contribution from the fuel abstraction reaction. Again, this result explains why the higher fuel concentration mixtures are more reactive. As temperature increases, Fig. 6b, there is a combination of $\dot{C}_2H_3/O_2$ and $\dot{H}/O_2$ systems controlling reactivity, particularly for the fuel-lean mixtures. This trend continues at the highest temperature, Fig. 6c, with the $\dot{H}+O_2 \rightleftarrows \dot{O}\dot{H}+\dot{O}$ H reaction the most significant for both equivalence ratios. Due to the higher pressure, there is also noticeable dependence on the pressure-dependent hydroperoxyl radical formation, a reaction not highlighted as important at the lower pressures of this study.

B. Pressure Dependence

Figures 7–10 show the effect of pressure on ignition delay time at the different equivalence ratios. As in the equivalence ratio study in the previous section, the simulations have been performed over an exaggerated temperature range (and, hence, ignition delay timescale). Examining the experimental data, there is a noticeable bifurcation with regard to pressure dependence, with the fuel-lean mixtures showing essentially zero dependence and the stoichiometric and fuel-rich mixtures exhibiting a more typical dependence, with higher pressures having higher reactivity. However, analyzing the data and simulations together over a large temperature scale, all equivalence ratios show the same general trend—significant pressure dependence at both low and high

Deleted: The equivalence ratio dependence at higher pressures, seen in Figs. 3 and 4, is very similar to that found at atmospheric pressure, where there is a significant dependence at lower temperatures and a minimal dependence at higher temperatures. Examining the dependence over the experimental temperature range in isolation, there is a noticeable increase in equivalence ratio dependence as the pressure increases. However, the simulations suggest that the temperature at which the reactivity of the different mixtures converges simply moves to a higher temperature as the pressure increases. Analogous behavior is visible in a typical alkane [7], where the temperature at which rich mixtures transition from most reactive to least reactive increases with elevated pressures. The characteristic is caused by the competition between the chain branching reaction

Deleted: $+O_2 \rightleftarrows$

Deleted: +

Deleted: H and the pressure-dependent, stabilization/propagation reaction

Deleted: $+O_2(+M) \rightleftarrows H$

Deleted: $_2(+M)$, forming the hydroperoxyl radical. At higher pressures, a higher temperature is required for the chain branching pathway to become the most significant. Therefore, the shift in hydrocarbon reactivity-controlling kinetics to the

Deleted: $/O_2$ system occurs at a higher temperature at 20 atm when compared to, for example, 1 atm.¶

Deleted: —

temperatures—but significantly less dependence at the intermediate temperatures, approximately in the range 1100–1400 K (i.e., the temperature range encompassing the experimental observations). In an attempt to explain the observed pressure dependence, the sensitivity analyses utilized to explain the observed equivalence ratio dependence are now plotted as a function of pressure in Figs. 11 and 12, for fuel-lean and fuel-rich mixtures, respectively.

Deleted:

Figure 11a shows the most-sensitive reactions controlling ignition for an equivalence ratio of 0.3 at a temperature of 1000 K and pressures of 1.0 and 22.0 atm. At this temperature, the sensitivities for both pressures are very similar with the only significant differences in the sensitivities of reactions $\dot{H}+O_2 \rightleftarrows \dot{O}\dot{H}+\dot{O}H$ and $C_2H_4+\dot{H}(+M) \rightleftarrows \dot{C}_2H_5(+M)$. The similarities in the sensitivities can be explained by examining a flux analysis performed at 20 percent fuel consumption. At this temperature, the relative consumption of the fuel and vinyl radicals is independent of pressure. At both pressures, the majority of fuel is consumed through $\dot{H}$-atom abstraction by hydroxyl radicals, followed by oxygen-atom addition reactions. The fate of the vinyl radical is also invariant with pressure, with consumption by molecular oxygen dominating, hence the large sensitivities depicted. However, the consumption of $\dot{H}$ atoms is significantly affected by pressure, arising to the differences presented in Fig. 11a. At the lower pressure, approximately 20% of the $\dot{H}$ atoms undergo chain branching through reactions with molecular oxygen. At elevated pressure, this reaction consumes only 5% of the $\dot{H}$ atoms, with the majority (>50%) undergoing a propagation reaction with molecular oxygen via the collisionally stabilized reaction to form hydroperoxyl radicals. $\dot{H}$-atom addition to ethylene to form ethyl radicals is of equal significance at both pressures, with the reaction consuming approximately 27% of the $\dot{H}$-atom concentration. The larger sensitivity at low pressure is due to the competition for $\dot{H}$ atoms with the chain branching molecular oxygen reaction.

As the temperature is increased to 1200 K, the results of the sensitivity analysis at different pressures start to exhibit significant differences, Fig. 11b. This particular temperature is in the middle of the regime where the majority of the experimental data were obtained, Fig. 7, with little effect of pressure visible. The model predictions in Fig. 7 show that at low pressure there is a more-pronounced effect of increasing temperature when compared to high pressures. Comparing the predicted ignition delay times at 1.2 atm at 1000 and 1200 K, the ignition delay time is reduced by approximately a factor of 140 at the higher temperature, whereas at 22 atm, this factor is only 22. It is evident from the sensitivity analysis at 1200 K that the hydrogen/oxygen sub-mechanism is more important at this temperature, with the chain branching reaction with molecular oxygen now the most dominant reaction affecting the reactivity of the low-pressure mixture. This reaction ($\dot{H}+O_2 \rightleftarrows \dot{O}+\dot{O}H$) has also a reasonable sensitivity at higher pressure but is still dominated by the vinyl plus molecular oxygen system. The larger promoting effect of temperature at lower pressure relative to higher pressure is related to the competition between chain branching and propagation in the H_2/O_2 system. This competition is reiterated by a flux analysis performed at 1200 K and 20 percent fuel consumption. At low pressure, 33% of hydrogen atoms react with molecular oxygen to undergo chain branching, with only 4% forming being stabilized to form hydroperoxyl radicals. At 22 atm, only 16% of the $\dot{H}$ atoms undergo chain branching, while 38% are consumed through the propagation pathway yielding the hydroperoxyl radical. The increased influence of hydrogen-oxygen chain branching at low pressure is accentuated as the oxygen atom produced is free to undergo another chain branching reaction through addition to the fuel, reproducing a $\dot{H}$ atom and a vinoxy radical. This reaction has a significantly larger sensitivity at lower pressure, Fig. 11b.

Deleted:

Deleted: increased considerably in

Deleted: significance

Deleted: Ḣ

Another interesting facet of the analysis depicted in Fig. 11b is the opposite sensitivity shown by vinoxy-radical decomposition to ketene and an $\dot{H}$ atom. At low pressure, this reaction promotes reactivity as it produces an $\dot{H}$ atom which leads to chain branching via $\dot{H}+O_2 \rightleftarrows \ddot{O}+\dot{O}H$. At elevated pressure (22 atm), this $\dot{H}$ atom predominantly

Deleted: .

undergoes propagation ($\dot{H}+O_2$ (+M) $\rightleftarrows H\dot{O}_2$ (+M)) which leads to the inhibiting effect as the decomposition competes with vinoxy radicals reacting with molecular oxygen to produce, among other products, hydroxyl radicals.

The reactivity at higher temperatures, Fig. 7, shows a similar pattern as for the lower temperatures, with the higher-pressure simulations being more reactive. This higher reactivity at higher pressure is indicative of the controlling kinetics being similar at both high and low pressure, with the larger reactivity simply resulting from a concentration effect. This argument is emphasized by the sensitivity results at 1400 K, Fig. 11c, which are very similar at both pressures, with the only significant difference being the considerably larger sensitivities to $\dot{H}+O_2 \rightleftarrows \dot{O}\dot{H}+\dot{O}H$ and $\dot{H}+O_2(+M) \rightleftarrows H\dot{O}_2(+M)$ at higher pressures, with the larger sensitivity arising from the competition between the two pathways. The two chain branching reactions, $\dot{H}+O_2 \rightleftarrows \dot{O}\dot{H}+\dot{O}H$ and $C_2H_4+\dot{O}\ \dot{O} \rightleftarrows CH_2CH\dot{O}+\dot{H}$ are the most important promoting reactions at both pressures. This pair of chain branching reactions was also the case at low pressures at 1200 K, but not at high pressure as the stabilization reaction between $\dot{H}$ atoms and molecular oxygen was limiting reactivity. However, at this elevated temperature, this reaction is less significant, a point illustrated by flux analysis, once again performed at 20 percent fuel consumption. Unlike at 1200 K, the main

Formatted: Not Superscript/ Subscript

Formatted: Subscript

Deleted:

consumption route for $\dot{H}$ atoms at 22 atm is now via the chain branching reaction with molecular oxygen, consuming 29%. The increased temperature enables this reaction to out compete the stabilization reaction which now accounts for only 23% of $\dot{H}$-atom consumption. This competition again results in both low- and high-pressure cases having very similar chemistry, namely subsequent chain branching reactions via hydrogen atom and molecular oxygen and fuel plus atomic oxygen. This similarity results in the more typical pressure dependence predicted at higher temperatures, where the higher concentrations of reactants leads to higher reactivity, Figs. 7 and 8.

As noted above, the experimental data show an increase in pressure dependence with increasing equivalence ratio. At stoichiometric and fuel-rich conditions, Figs. 9 and 10, there is significant pressure dependence, particularly at ϕ = 2.0 (Fig. 10). The model predicts very similar reactivity trends at both fuel-lean and fuel-rich conditions, with the reactivity not converging to the same degree at ϕ = 2.0 compared to ϕ = 0.3 in the temperature range 1100 – 1400 K. To aid the discussion, the results of the sensitivity analysis have also been plotted up as a function of pressure for the fuel-rich mixture, Fig. 12. This figure is very similar to Fig. 11 at both high and low temperature, signifying that the pressure dependence is essentially independent of equivalence ratio at these temperature extremes. This zero dependence on ϕ in temperature range 1100–1400 K is also evident from Figs. 2 and 4, with very similar behavior predicted by the model at these conditions.

At fuel-lean conditions, it was found that the convergence of reactivity at intermediate temperatures was due to the higher promoting effect of temperature at low pressure arising from the increased importance of $\dot{H}+O_2 \rightleftarrows \dot{O}\dot{H}+\dot{O}$ H and further subsequent chain branching from $C_2H_4+\dot{O}\dot{O} \rightleftarrows CH_2CH\dot{O}\dot{O}+\dot{H}$. These reactions are of a lesser importance at higher pressure due to the competition of the stabilization reaction to form the hydroperoxyl radical. This result is also the case at fuel-rich conditions, with reactivity increasing more rapidly with increasing

Deleted: CH_2CH

temperature at lower pressure than at higher pressure. However, the efficacy of the $\dot{H}+O_2 \rightleftarrows \dot{O}H+\dot{O}$ H reaction is

reduced due to the higher fuel concentration which consumes hydrogen atoms through abstraction and addition reactions. By examining Fig. 12b, this fact is highlighted as vinyl-radical chemistry is still dominant at both pressures (1 and 22 atm), with a reduced sensitivity to the hydrogen/oxygen and ethylene/oxygen atom systems, particularly at higher pressure. The increased importance of the hydrogen-atom reactions with ethylene, and the subsequent reduction in the importance of $\dot{H}+O_2 \rightleftarrows \dot{O}H+\dot{O}$ H and $C_2H_4+\dot{O}\dot{O} \rightleftarrows CH_2CH\dot{O}\dot{O}+H\dot{H}$, results in the experimentally observed pressure dependence for stoichiometric and fuel-rich conditions, Figs. 9 and 10.

Deleted:

Deleted: CH_2CH

C. Comparison with Dilute Archival Data

A number of dilute ethylene data from past literature studies were compiled and are compared in Figs. 13–15, along with the predictions of the improved C_4 mechanism. All of the data are from mixtures with a composition of 1.0% C_2H_4, 3.0% O_2, and 96.0% Ar; equivalence ratio of 1.0; and, average pressures of 1.2 to 2.7 atm. This mixture was selected for comparison herein because it was utilized in at least five different shock-tube studies from the literature. The experimental data depicted in Fig. 13, at an average pressure of 1.2 atm, from Davidson and Hanson [35] and Kalitan *et al.* [36] show good agreement with each other, while the data from Brown and Thomas [37] tend to lie below the two other data sets. The mechanism agrees excellently with the data from Davidson and Hanson and Kalitan *et al.* in Fig. 13.

There is good agreement between all four sources in Fig. 14, at an average pressure of 2.1 atm, as well as for the three data sets in Fig. 15, at an average pressure of 2.7 atm. The data in Fig. 14 include measurements from Davidson and Hanson [35], Brown and Thomas [37], Hidaka et al. [38], and the recent study of Saxena *et al.* [39]. The mechanism predicts a slightly lower activation energy than what the data suggest in Fig. 14, leading to an over-

Deleted: Brown and Thomas [37], Davidson and Hanson [35],

prediction of ignition delay time at higher temperatures. However, the agreement between model and data is excellent in Fig. 15. The good agreement amongst multiple data sets from different shock tubes in Figs. 13–15 lends confidence to the integrity of the literature database for the 96% Ar, $\phi = 1$ mixture. This mixture would therefore serve as an excellent target for future mechanism development.

IV. Model Comparisons and Validation

In light of some of the pressure and equivalence ratio characteristics seen in the present study for ethylene over the intermediate temperature range covered (1000 – 1400 K), it is insightful to compare the data from Part 1 to other chemical kinetics models, including an earlier version of the authors' mechanism, C4_49. This earlier version of the detailed mechanism is available at http://c3.nuigalway.ie/naturalgas3.html. Two other mechanisms include the San Diego Mechanism (http://web.eng.ucsd.edu/mae/groups/combustion/mechanism.html) and the USC 2.0 mechanism, available at http://ignis.usc.edu/Mechanisms/USC-Mech%20II/USC_Mech%20II.htm.

Figure 16 presents the predictions of the various mechanisms in comparison with the present one for the ignition delay time data near 1 atm, for each of the 4 equivalence ratios tested in Kopp *et al.* [1]. For all four values of ϕ in Fig. 16, the current mechanism and the San Diego mechanism are in agreement with each other, and both seem to match the experimental results the best, particularly for the stoichiometric and fuel-rich conditions. This result is a dramatic improvement over the C4_49 version for all cases. The USC 2.0 mechanism tends to over-predict the ignition delay times by a factor of 5 or more at fuel-lean conditions and a factor of two of more at $\phi = 1$. At a pressure near 10 atm, all of the mechanisms perform much better than at the lower pressure, as seen in Fig. 17. Again, there is good agreement between the present model and the San Diego mechanism. The biggest improvement over the earlier version of the model is in the $\phi = 0.3$ results, where the original prediction (as well as that of USC Mech 2.0) over-predicts the ignition delay time and underestimated the temperature dependence.

Comparisons against the relatively recent data set of Saxena *et al.* (using OH* as the ignition diagnostic) [39] were also performed. Figure 18 shows some selected comparisons for their shock-tube results using C_2H_4-O_2 mixtures diluted in 93% Argon by volume. All four mechanisms show very good agreement with the $\phi = 1$ data near 2 atm (Fig. 18a). Each mechanism shows good agreement with each other at $\phi = 1$ and 9.3 atm (Fig. 18b), but collectively under-predict the ignition delay times by about a factor of two (although there is better agreement at lower temperatures for most of the models except the present one). For the fuel-rich Saxena *et al.* data ($\phi = 3$), there

Deleted: 8

is fair agreement at the lower temperature of 2.1 atm (Fig. 18c), but the models collectively under-predict the ignition delay times at the higher pressure of 18 atm (Fig. 18d) by about a factor of two. The experimental results in Fig. 18 when combined with the present data certainly test the limits of the kinetics models, and while there is generally good agreement between the data and the updated mechanism, further improvements can be made.

Of course, a more thorough test of the kinetics model is to use data from experiments other than ignition delay times. Such comparisons were made throughout the development of the current version of the mechanism. Laminar flame speed data from Egolfoupolos *et al.* [40], Hassan *et al.* [41], and Jomass *et al.* [42] are available for ethylene-air mixtures at pressures from 1 to 5 atm. Un-stretched, unburned gas laminar flame speeds were calculated using Chemkin Pro [2]; solutions converged to GRAD and CURV values of 0.02 (> 800 grid points) utilizing mixture-averaged transport equations including thermal diffusion effects. Figure 19 compares the model predictions to the three sets of flame speed data, with very good agreement over the range of equivalence ratios available. Near ϕ = 1.2, the Egolfoupolos *et al.* [40] data appear to be about 5–10 cm/s higher than the other data sets at 1 atm, and the model tends to agree with the slower data sets.

Deleted: -

Additional datasets used in the improvement of the ethylene oxidation chemistry but not included herein due to space requirements include the 59-atm flow reactor speciation data from Lopez *et al.* [43]. Three sources of jet-stirred reactor data were also used for comparison, namely those of Dagaut *et al.* [44], Le Cong *et al.* [45], and Jallais *et al.* [46]. Finally, the shock-tube ignition delay time data from Penyazkov *et al.* [47] were also modeled, the results of which are provided in Kopp et al. [1].

V. Conclusions

A detailed chemical kinetics model under continuous development in the authors' laboratory has been improved to better agree with the results of ignition delay time experiments obtained by the authors and presented in a different paper. The C_2H_4-air mixtures covered a range of pressures from about 1 to 25 atm, equivalence ratios from 0.3 to 2.0, and temperatures between 1000 and 1400 K. The original version of the mechanism was shown to be deficient in predicting the ignition delay times over this range of temperature, where the data exhibited trends such as zero pressure dependence at fuel-lean conditions and a decreasing effect of ϕ at higher temperatures. Improvements to the model resulted in significantly better agreement in these respects, although the model still tends to over-predict ignition delay times at low pressures for the fuel-lean cases. In general, the best agreement between model and data was seen at stoichiometric and fuel-rich conditions, particularly for the higher pressures (10+ atm).

Much discussion was presented to describe the interesting chemical kinetics that occurs within the temperature, pressure, and stoichiometry space covered in this study. Detailed ignition sensitivity and species flux analyses over the range of P, T, and ϕ space proved invaluable in this regard. Arguably, this is the first paper to correctly identify and model the observed behavior, which was shown herein to also be evident in other data from the literature.

Comparisons with two other chemical kinetics models showed that the current study can be used to make further improvements in the mechanisms from other groups and that the ignition trends observed were certainly not obvious given the level of disagreement between the other models and the data at the conditions of the present study. Other data sets including shock-tube ignition delay times and laminar flame speeds available in the literature were compared with the predictions of the current model, with mostly fair agreement overall, particularly in the prediction of the temperature behavior and the gross effect of equivalence ratio, pressure, and level of dilution. While further improvement is still needed, the current version is much improved over the original one as a result of the experiments and modeling presented in Kopp et al. [1] and the present paper, respectively.

Acknowledgments

The work at NUIG were supported by the Saudi Arabian Oil Company. The work at TAMU were supported primarily by the National Science Foundation, Grant Number CBET-0832561.

Deleted: efforts

Deleted: efforts

References

[1] Kopp, M. M., Donato, N. S., Petersen, E. L., Metcalfe, W. K., Burke, S. M., and Curran, H. J., "Ignition and Oxidation of Ethylene-Air Mixtures at Elevated Pressures, Part 1: Experimental Results," *Journal of Propulsion and Power*, submitted.

[2] CHEMKIN-PRO, Release 15101, 2010, Reaction Design: San Diego.

[3] Ó Conaire, M., Curran, H. J., Simmie, J. M., Pitz, W. J., and Westbrook, C. K., "A Comprehensive Modeling Study of Hydrogen Oxidation," *International Journal of Chemical Kinetics*, Vol. 36, 2004, pp. 603–622.

[4] Petersen, E. L., Kalitan, D. M., Simmons, S., Bourque, G., Curran, H. J., and Simmie, J. M., "Methane/Propane Oxidation at High Pressures: Experimental and Detailed Chemical Kinetic Modeling," *Proceedings of the Combustion Institute*, Vol. 31, 2007, pp. 447–454.

[5] Healy, D., Curran, H. J., Simmie, J. M., Kalitan, D. M., Petersen, E. L., and Bourque, G., "Methane/Propane Mixture Oxidation at High Pressures and at High, Intermediate and Low Temperatures," *Combustion and Flame*, Vol. 155, 2008, pp. 451–461.

[6] Healy, D., Curran, H. J., Simmie, J. M., Kalitan, D. M., Zinner, *C.* M., Barrett, A. B., Petersen, E. L., and Bourque, G., "Methane/Ethane/Propane Mixture Oxidation at High Pressures and at High, Intermediate and Low Temperatures," *Combustion and Flame*, Vol. 155, 2008, pp. 441–448.

[7] Healy, D., Donato, N. S., Aul, C. J., Petersen, E. L., Zinner, C. M., Bourque, G., and Curran, H. J., "n-Butane: Ignition Delay Measurements at High Pressure and Detailed Chemical Kinetic Simulations," *Combustion and Flame*, Vol. 157, 2010, pp. 1526–1539.

[8] Healy, D., Donato, N. S., Aul, C. J., Petersen, E. L., Zinner, C. M., Bourque, G., and Curran, H. J., "Isobutane: Ignition Delay Measurements at High Pressure and Detailed Chemical Kinetic Simulations," *Combustion and Flame*, Vol. 157, 2010, pp. 1540–1551.

[9] Donato, N., Aul, C., Petersen, E., Zinner, C., Curran, H., and Bourque, G., "Ignition and Oxidation of 50/50 Butane Isomer Blends," *Journal of Engineering for Gas Turbines and Power*, Vol. 132, No. 5, 2010, pp. 051502–9.

[10] Healy, D., Kopp, M. M., Polley, N. L., Petersen, E. L., Bourque, G., and Curran, H. J., "Methane/n-Butane Ignition Delay Measurements at High Pressure and Detailed Chemical Kinetic Simulations," *Energy & Fuels*, Vol. 24, 2010, pp. 1617–1627.

[11] Healy, D., Kalitan, D. M., Aul, C. J., Petersen, E. L., Bourque, G., and Curran, H. J., "Oxidation of C1–C5 Alkane Quinternary Natural Gas Mixtures at High Pressures," *Energy & Fuels*, Vol. 24, 2010, pp. 1521–1528.

[12] Metcalfe, W. K., Burke, S. M., Ahmed, S. S. and Curran, H. J., "A Hierarchical and Comparative Kinetic Modeling Study of C_1–C_2 Hydrocarbon and Oxygenated Fuels", Int. J. Chem. Kinet. Vol. 45, No. 10, 2013, pp. 638–675.

[13] http://garfield.chem.elte.hu/Burcat/BURCAT.THR

[14] Kéromnès, A., Metcalfe, W. K., Donohoe, N., Curran, H. J., and Pitz, W. J., "Detailed Chemical Kinetic Model for H_2 and H_2/CO (Syngas) Mixtures at Elevated Pressure," *7th US Nat. Meeting of the Comb. Inst, Atlanta*, 21-23/03/2011.

[15] Kéromnès, A., Metcalfe, W. K., Donohoe, N. Das, A. K., Sung, C. J., Herzler, J., Naumann, C., Griebel, P., Mathieu, O., Petersen, E. L., Pitz, W. J., and Curran, H. J., "Detailed Chemical Kinetic Model for Hydrogen and Syngas Mixtures at Elevated Pressure," *Combustion and Flame*, Vol/ 160, 2013, pp. 995–1011.

[16] Lowry, W., de Vries, J., Krejci, M., Petersen, E., Serinyel, Z., Metcalfe, W., Curran, H., and Bourque, G., "Laminar Flame Speed Measurements and Modeling of Pure Alkanes and Alkane Blends at Elevated Pressures," *Journal of Engineering for Gas Turbines and Power-Transactions of the ASME*, Vol. 133, No. 9, 2011, pp. 091501-9.

[17] Aul, C. J., Metcalfe, W. K., Burke, S. M., Curran, H. J., and Petersen, E. L., submitted to Combustion and Flame 2012

[18] Laskin, A., Wang, H., and Law, C. K., "Detailed Kinetic Modeling of 1,3-Butadiene Oxidation at High Temperatures," *International Journal of Chemical Kinetics,* Vol. 32, 2000, pp. 589–614.

Formatted: English (U.S.)

Deleted: submitted.¶

Deleted: ¶

Formatted: English (U.S.)

Deleted: Metcalfe, W. K., Burke, S. M., Aul, C. J., Petersen, E. L., and Curran, H. J., "A Detailed Chemical Kinetic Modelling and Experimental Study of C_1–C_2 Hydrocarbons," European Combustion Meeting, June 29th - July 1st 2011, Cardiff, Wales.¶

Formatted: Font: 9 pt

[19] Davis, S. G., Law, C. K., and Wang. H., "Propene Pyrolysis and Oxidation Kinetics in a Flow Reactor and Laminar Flames," *Combustion and Flame*, Vol. 119, 1999, pp. 375–399.

[20] Smith G. P., Golden D. M., Frenklach M., Moriarty N. W., Eiteneer B., Goldenberg M., Bowman C. T., Hanson R. K., Song S., Gardiner, Jr., W. C., Lissianski V. V., and Qin Z. http://www.me.berkeley.edu/gri_mech/

[21] Wang, H., You, X., Joshi, A. V., Davis, S. G., Laskin, A., Egolfopoulos, F., and Law, C. K., "USC Mech Version II. High-Temperature Combustion Reaction Model of H_2/CO/C_1–C_4 Compounds," 2007. http://ignis.usc.edu/USC_Mech_II.htm.

[22] Baulch, D. L.; Bowman, C. T.; Cobos, C. J.; Cox, R. A.; Just, T.; Kerr, J. A.; Pilling, M. J.; Stocker, D.; Troe, J.; Tsang, W.; Walker, R. W.; Warnatz, J., "Evaluated Kinetic Data for Combustion Modeling: Supplement II." Journal of Physical and Chemical Reference Data 2005, 34 (3), 757–1397.

[23] Nguyen, T. L., Vereecken, L., Hou, X. J., Nguyen, M. T., and Peeters, J., "Potential Energy Surfaces, Product Distributions and Thermal Rate Coefficients of the Reaction of $O(^3P)$ with $C_2H_4(X^1A_g)$: A Comprehensive Theoretical Study," *Journal of Physical Chemistry A,* Vol. 109, 2005, pp. 7489–7499.

[24] Vasu, S. S., Hong, Z., Davidson, D. F., Hanson, R. K., and Golden, D. M., "Shock Tube/Laser Absorption Measurements of the Reaction Rates of OH with Ethylene and Propene," *Journal of Physical Chemistry A*, Vol. 114, 2010, pp. 11529–11537.

[25] Senosiain, J. P., Klippenstein, S. J., and Miller, J. A., "Reaction of Ethylene with Hydroxyl Radicals: A Theoretical Study," *Journal of Physical Chemistry A*, Vol. 110, 2006, pp. 6960–6970.

[26] Baulch, D. L., Cobos, C. J., Cox, R. A., Frank, P., Hayman, G., Just, Th., Kerr, J. A., Murrells, T., Pilling, M. J., Troe, J., Walker, R. W., and Warnatz, J., "Evaluated kinetic data for combusion modelling. Supplement I," *Journal of Physical Chemistry Reference Data*, Vol. 23, 1994, pp. 847–1033.

[27] Mebel, A. M., Diau, E. W. G., Lin, M. C., and Morokuma, K., "Ab Initio and RRKM Calculations for Multichannel Rate Constants of the $C_2H_3 + O_2$ Reaction," *Journal of the American Chemical Society*, Vol. 118, 1996, pp. 9759–9771.

[28] Chang, A. Y., Bozzelli, J. W., and Dean, A. M., "Kinetic Analysis of Complex Chemical Activation and Unimolecular Dissociation Reactions using QRRK Theory and the Modified Strong Collision Approximation," *Zeitschrift für Physikalische Chemie*, Vol. 214, No. 11, 2000, pp. 1533–1568.

[29] Klippenstein, S. J., Georgievskii, Y., Miller, J. A., Nummela, J. A., Carpenter, B. K., and Westmoreland, P. R., "Vinyl + O_2: A Complete Theoretical Treatment," *Proceedings of the Third Joint Meeting of the U. S. Sections of The Combustion Institute*, 2003.

Deleted: -

[30] Lopez J. G., Rasmussen, C. L., Alzueta, M. U., Gao Y., Marshall, P., and Glarborg P., "Experimental and Kinetic Modeling Study of C_2H_4 Oxidation at High Pressure," *Proceedings of the Combustion Institute*, Vol. 32, 2009, pp. 367–375.

[31] Marinov, N., Pitz, W., Westbrook, C., Vincitore, A., Castaldi, M., Senkan, S., and Melius, C., "Aromatic and Polycyclic Aromatic Hydrocarbon Formation in a Laminar Premixed n-Butane Flame," *Combustion and Flame*, Vol. 114, No. 1–2, 1998, pp. 192–213.

[32] Dagaut, P., Voisin, D., Cathonnet, M., McGuinness, M., and Simmie, J., "The Oxidation of Ethylene Oxide in a Jet-Stirred Reactor and Its Ignition in Shock Waves," *Combustion and Flame*, Vol. 106, No. 1–2, 1996, pp. 62–68.

[33] Senosiain, J. P., Klippenstein, S. J., and Miller, J. A., "Pathways and Rate Coefficients for the Decomposition of Vinoxy and Acetyl Radicals," *Journal of Physical Chemistry A,* Vol. 110, 2006, pp. 5772–5781.

[34] Troe, J., "Predictive Possibilities of Unimolecular Rate Theory," *Journal of Physical Chemistry*, Vol. 83, No. 1, 1979, pp. 114–126.

[35] Davidson, D. F. and Hanson R. K., "Fundamental Kinetics Database Utilizing Shock Tube Measurements," Mechanical Engineering Department, Stanford University, Vol. 1, 2005, pp. 1–75.

[36] Kalitan, D. M., Hall, J. M., and Petersen, E. L., "Ignition and Oxidation of Ethylene-Oxygen-Diluent Mixtures with and Without Silane," *Journal of Propulsion and Power*, Vol. 21, No. 6, 2005, pp. 1045–1056.

[37] Brown, C. and Thomas, C., "Experimental Studies of Shock-Induced Ignition and Transition to Detonation in Ethylene and Propane Mixtures," *Combustion and Flame*, Vol. 117, No. 4, 1999, pp. 861–870.

[38] Hidaka, Y., Kataoka, T., and Suga, M., "A Shock-Tube Investigation of Ignition in Ethylene- Oxygen- Argon Mixtures," *Bulletin of the Chemical Society of Japan*, Vol. 47, No. 9, 1974, pp. 2166–2170.

[39] Saxena, S., Kahandawala, M. S. P., and Sidhu, S. S., "A Shock Tube Study of Ignition Delay in the Combustion of Ethylene," *Combustion and Flame*, Vol. 158, 2011, pp. 1019-1031.

[40] Egolfopoulos, F. N., Zhu, D. L., and Law, C. K., "Experimental and Numerical Determination of Laminar Flame Speeds: Mixtures of C_2-Hydrocarbons with Oxygen and Nitrogen," *Proceedings of the Combustion Institute*, Vol. 23, 1991, pp. 471-478.

[41] Hassan, M. I., Aung, K. T., Kwon, O. C., and Faeth, G. M., "Properties of Laminar Premixed Hydrocarbon/Air Flames at Various Pressures," *Journal of Propulsion and Power*, Vol. 14, No. 4, 1998, pp. 479-488.

[42] Jomaas, G., Zheng, X. L., Zhu, D. L., and Law, C. K., "Experimental Determination of Counterflow Ignition Temperatures and Laminar Flame Speeds of C_2-C_3 Hydrocarbons at Atmospheric and Elevated Pressures," *Proceedings of the Combustion Institute*, Vol. 30, 2005, pp. 193-200.

[43] Lopez, J. G., Rasmussen, C. L., Alzueta, M. U., Gao, Y., Marshall, P., and Glarborg, P., "Experimental and Kinetic Modeling Study of C_2H_4 Oxidation at High Pressure," *Proceedings of the Combustion Institute*, Vol. 32, 2009, pp. 367-375.

[44] Dagaut, P., Boettner, J. C., and Cathonnet, M., "Ethylene Pyrolysis and Oxidation: A Kinetic Modeling Study," *International Journal of Chemical Kinetics*, Vol. 22, No. 6, 1990, pp. 641–664.

[45] Le Cong, T., Bedjanian, E., and Dagaut, P., "Oxidation of Ethylene and Propene in the Presence of CO_2 and H_2O: Experimental and Detailed Kinetic Modeling Study," *Combustion Science and Technology*, Vol. 182, 2010, pp. 333-349.

[46] Jallais, S., Bonneau, L., Auzanneau. M., Naudet, V., and Bockel-Macal, S., "An Experimental and Kinetic Study of Ethene Oxidation at a High Equivalence Ratio," *Industrial Engineering Chemistry Research*, Vol. 41, No. 23, 2002, pp. 5659-5667.

[47] Penyazkov, O. G., Sevrouk, K. L., Tangirala, V., and Joshi, N., "High-Pressure Ethylene Oxidation Behind Reflected Shock Waves," *Proceedings of the Combustion Institute*, Vol. 32, 2009, pp. 2421–2428.

[48] Knyazev, V. D., Bencsura,, A., Stoliarov, S. I., and Slagle, I. R., "Kinetics of the $C_2H_3 + H_2 \rightleftarrows H + C_2H_4$ and $CH_3 + H_2 \rightleftarrows H + CH_4$ Reactions," *Journal of Physical Chemistry*, Vol. 100, 1996, pp. 11346–11354.

[49] Butler, J. E., Fleming, J. W., Goss, L. P., and Lin, M. C., "Kinetics of CH Radical Reactions Important to Hydrocarbon Combustion Systems," *American Chemistry Society Symposium Series*, Vol. 134, 1980, pp. 397.

[50] Miller, J. A. and Klippenstein, S. J., "The $H+C_2H_2(+M) \leftrightarrow C_2H_3(+M)$ and $H+C_2H_2(+M) \leftrightarrow C_2H_5(+M)$ reactions: Electronic structure, variational transition-state theory, and solutions to a two-dimensional master equation," *Physical Chemistry Chemical Physics*, Vol. 6, 2004, pp. 1192–1202.

Table 1. Updated Ethylene sub mechanism. Units: $cm^3\ mol^{-1}\ s^{-1}\ cal^{-1}$.

Reaction	*A*	*n*	*Ea*	*Ref.*
$\dot{C}_2H_3+\dot{H}$(+M)<=>C_2H_4(+M)	6.08E+12	0.3	280	[20]
LOW 1.40E+30 -3.86E+00 3.32E+03				
TROE 7.82E-01 2.08E+02 2.66E+03 6.10E+03				
H_2/2.0/ H_2O/6.0/ AR/0.7/ CO/1.5/ CO_2/2.0/ CH_4/2.0/ C_2H_6/3.0/ HE/0.7/				
C_2H_4(+M)<=>$H_2+H_2C\dot{C}$(+M)	8.00E+12	0.4	88770	[20], *see text*
LOW 7.00E+50 -9.31E+00 9.99E+04				
TROE 7.35E-01 1.80E+02 1.04E+03 5.42E+03				
H_2/2.0/ H_2O/6.0/ CH_4/2.0/ CO/1.5/ CO_2/2.0/ C_2H_6/3.0/ AR/0.7/				
$C_2H_4+\dot{H}$<=>$\dot{C}_2H_3+H_2$	5.07E+07	1.9	12950	[48]
$C_2H_4+\dot{O}$<=>$\dot{C}H_3+H\dot{C}O$	7.45E+06	1.9	183	[22] , *see text*
$C_2H_4+\dot{O}$<=>$\dot{C}H_2CHO+\dot{H}$	6.10E+06	1.9	183	[22], *see text*
$C_2H_4+\dot{O}H$<=>$\dot{C}_2H_3+H_2O$	2.23E+04	2.7	2216	[24]
$C_2H_4+\dot{O}H$<=>$\dot{C}H_3+CH_2O$ (1 atm)	1.78E+05	1.7	2061	[25]
$C_2H_4+\dot{O}H$<=>$CH_3CHO+\dot{H}$(1 atm)	2.38E-02	3.9	1723	[25]
$C_2H_4+\dot{O}H$<=>$C_2H_3OH+\dot{H}$(1 atm)	3.19E+05	2.2	5256	[25]
$C_2H_4+\dot{O}H$<=>p$\dot{C}_2H_4OH$ (1 atm)	2.56E+36	-7.8	6946	[25]
$C_2H_4+\dot{C}H_3$<=>$\dot{C}_2H_3+CH_4$	6.62E+00	3.7	9500	[22]
$C_2H_4+O_2$<=>$\dot{C}_2H_3+H\dot{O}_2$	4.22E+13	0	57623	[22]
$C_2H_4+CH_3\dot{O}$<=>$\dot{C}_2H_3+CH_3OH$	1.20E+11	0	6750	[22]
$C_2H_4+CH_3\dot{O}_2$<=>$\dot{C}_2H_3+CH_3O_2H$	8.59E+00	3.8	27132	*Est.*
$C_2H_4+C_2H_5\dot{O}_2$<=>$\dot{C}_2H_3+C_2H_5O_2H$	8.59E+00	3.8	27132	*Est.*
$C_2H_4+CH_3C\dot{O}_3$<=>$\dot{C}_2H_3+CH_3CO_3H$	1.13E+13	0	30430	[26]
$C_2H_4+H\dot{O}_2$<=>$C_2H_4O1\text{-}2+\dot{O}OH$	5.58E+11	0	17190	[26], *see text*
$\dot{C}H+CH_4$<=>$C_2H_4+\dot{H}$	6.00E+13	0	0	[49]
$\dot{C}H_2(S)+\dot{C}H_3$<=>$C_2H_4+\dot{H}$	2.00E+13	0	0	*Est.*
C_2H_2+H(+M)<=>C_2H_3(+M)	1.71E+10	1.3	2709	[50]
LOW 6.35E+31 -4.66E+00 3.78E+03				
TROE 7.88E-01 -1.02E+04 1.00E-30				
H_2/2/ H_2O/6/ AR/0.7/ CO/1.5/ CO_2/2/ CH_4/2/ C_2H_6/3/ HE/0.7/				
$C_2H_3+O_2$<=>$CH_2O+H\dot{C}O$	1.70E+29	-5.3	6503	[31]
$\dot{C}_2H_3+O_2$<=>$\dot{C}H_2CHO+\dot{O}$	7.00E+14	-0.6	5262	[31]
$\dot{C}_2H_3+O_2$=>$\dot{H}+CO+CH_2O$	5.19E+15	-1.3	3313	[31], *see text*
$\dot{C}H_3+\dot{C}_2H_3$<=>$CH_4+C_2H_2$	3.92E+11	0	0	[22]
$\dot{C}_2H_3+\dot{H}$<=>$C_2H_2+H_2$	9.00E+13	0	0	[22]
$\dot{C}_2H_3+\dot{H}$<=>H_2CC+H_2	6.00E+13	0	0	*Est.*
$\dot{C}_2H_3+\dot{O}H$<=>$C_2H_2+H_2O$	3.01E+13	0	0	[22]

Deleted: C...H ... [1]
Deleted: C ... [2]
Deleted: H...C ... [2]
Deleted: O...C...C ... [3]
Deleted: O...C...H ... [4]
Deleted: O...C ... [5]
Deleted: O...C ... [6]
Deleted: O...H ... [7]
Deleted: O...H ... [8]
Deleted: O...C ... [9]
Deleted: C...C ... [10]
Deleted: C...O ... [11]
Deleted: O...C ... [12]
Deleted: O...C ... [13]
Deleted: O...C ... [14]
Deleted: O...C ... [15]
Deleted: O ... [16]
Deleted: C...H ... [16]
Deleted: C...C...H ... [17]
Deleted: C ... [18]
Deleted: C...C...O ... [18]
Deleted: C...H ... [19]
Deleted: C...C ... [20]
Deleted: C...H ... [21]
Deleted: C...H ... [22]
Deleted: C...O ... [23]

$\dot{C}_2H_3+\dot{C}_2H_3<=>C_2H_2+C_2H_4$	9.60E+11	0	0	[22]
$CH_2CHO(+M)<=>CH_2CO+\dot{H}(+M)$	1.43E+15	-0.1	45600	[33], *see text*
LOW 6.00E+29 -3.80E+00 4.34E+04				
TROE 9.85E-01 3.93E+02 9.80E+09 5.00E+09				
$CH_2CHO(+M)<=>\dot{C}H_3+CO(+M)$	2.93E+12	0.3	40300	[33]
LOW 9.52E+33 -5.07E+00 4.13E+04				
TROE 7.13E-17 1.15E+03 4.99E+09 1.79E+09				
$C_2H_4+\dot{H}(+M)<=>\dot{C}_2H_5(+M)$	9.56E+08	1.5	1355.0	[17]
LOW 1.42E+39 -6.64 5769.0				
TROE -5.690E-01 2.99E+02 9.15E+03 1.52E+02				
H_2/2.0/ H_2O/6.0/ CH_4/2.0/ CO/1.5/ CO_2/2.0/ C_2H_6/3.0/ AR/0.7				

Deleted: C

Deleted: C

Deleted: H

Deleted: C

Deleted: H

Deleted: C

Table 2. Flux of selected species at 1 atm and 1000 K, 20 percent fuel consumption.

	ϕ = 0.3		ϕ = 2.0	
Reaction	**%**	**mol cm^{-3} s^{-1}**	**%**	**mol cm^{-3} s^{-1}**
C_2H_4 Consumption				
$C_2H_4+\dot{O}H<=>\dot{C}_2H_3+H_2O$	44	1.11E-05	40	1.50E-03
$C_2H_4+\dot{H}(+M)<=>\dot{C}_2H_5(+M)$	16	4.05E-06	11	4.30E-04
$C_2H_4+\dot{O}<=>\dot{C}H_3+H\dot{C}O$	15	3.76E-06	15	5.68E-04
$C_2H_4+\dot{O}<=>\dot{C}H_2CHO+\dot{H}$	15	3.76E-06	15	5.68E-04
$C_2H_4+\dot{C}H_3<=>\dot{C}_2H_3+CH_4$	-	-	7	2.60E-04
$C_2H_4+\dot{H}<=>\dot{C}_2H_3+H_2$	-	-	6	2.13E-04
C_2H_3 Consumption				
$\dot{C}_2H_3+O_2<=>CH_2CHO+\dot{O}$	51	6.01E-06	54	1.07E-03
$\dot{C}_2H_3+O_2<=>CH_2O+H\dot{C}O$	38	4.53E-06	22	4.23E-04
$\dot{C}_2H_3+O_2 =>\dot{H}+CO+CH_2O$	10	1.19E-06	9	1.68E-04
C_2H_5 Consumption	-	-		
$\dot{C}_2H_5+O_2<=>C_2H_4+H\dot{O}_2$	78	3.23E-06	27	1.28E-04
$\dot{C}_2H_5+HO_2<=>C_2H_5\dot{O}+\dot{O}H$	11	4.68E-07	22	1.07E-04
$2\dot{C}H_3<=>\dot{H}+\dot{C}_2H_5$	-	-	20	9.38E-05
$C_3H_8(+M)<=>\dot{C}H_3+\dot{C}_2H_5(+M)$	-	-	17	7.90E-05
H Consumption	-	-		
$C_2H_4+H(+M)<=>\dot{C}_2H_5(+M)$	27	4.05E-06	15	4.30E-04
$\dot{H}+O_2<=>\dot{O}+\dot{O}H$	20	2.94E-06	9	2.80E-04
$CH_2O+\dot{H}<=>H\dot{C}O+H_2$	18	2.70E-06	25	7.31E-04
$HO_2+\dot{H}<=>2\dot{O}H$	13	1.99E-06	15	4.31E-04
$\dot{H}+O_2(+M)<=>H\dot{O}_2(+M)$	9	1.40E-06		
$C_2H_4+\dot{H}<=>\dot{C}_2H_3+H_2$	-	-	7	2.13E-04
$CH_2CO+\dot{H}<=>H\dot{C}CO+H_2$	-	-	6	1.86E-04

Deleted: O…C ... [24]
Deleted: H…C ... [25]
Deleted: O…C…C ... [26]
Deleted: O…C…H ... [27]
Deleted: C…C ... [28]
Deleted: H…C ... [29]
Deleted: C_O ... [30]
Deleted: C_C ... [31]
Deleted: C_H ... [32]
Deleted: C_O ... [33]
Deleted: C_O…O ... [34]
Deleted: C…H…C ... [35]
Deleted: C…C ... [36]
Deleted: C
Deleted: H…O…O ... [37]
Deleted: H…C ... [38]
Deleted: H…O ... [39]
Deleted: H…O ... [40]
Deleted: H…C ... [41]
Deleted: H…C ... [42]

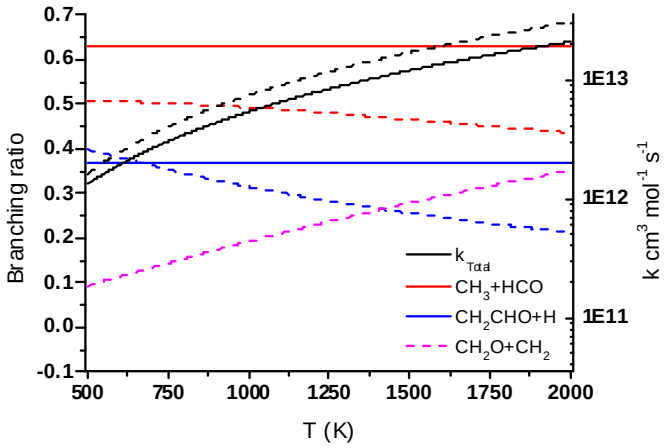

Figure 1: k_{Total} and branching ratio for the C_2H_4+O reaction. Solid line – Baulch *et al.* [22], dashed line – Nguyen [23].

Deleted: [22]

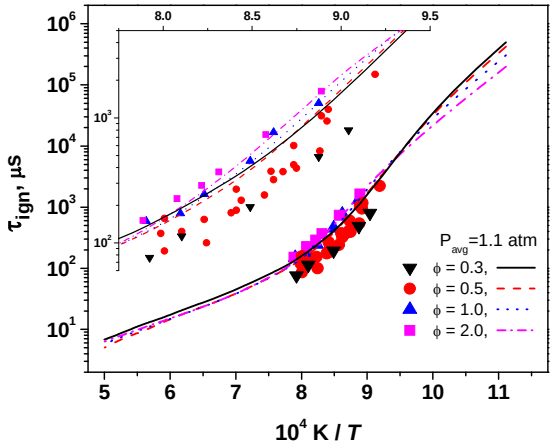

Figure 2. Ignition delay time data and modeling for P_{avg} = 1.1 atm showing equivalence ratio dependence at ϕ = 0.3, 0.5, 1.0, and 2.0. Symbols are experimental data, lines are current model simulations.

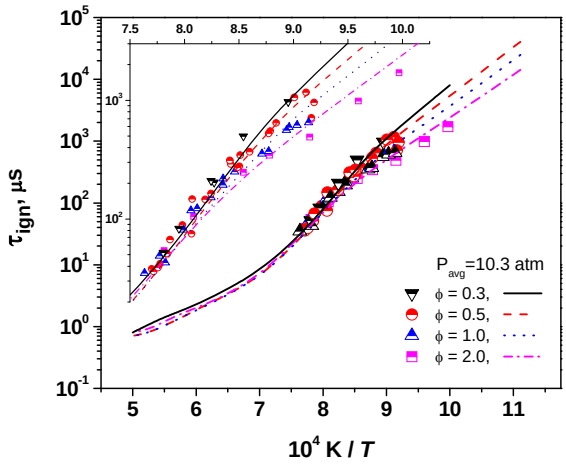

Figure 3. Ignition delay time data and modeling for P_{avg} = 10.3 atm showing equivalence ratio dependence at ϕ = 0.3, 0.5, 1.0, and 2.0. Symbols are experimental data, lines are current model simulations.

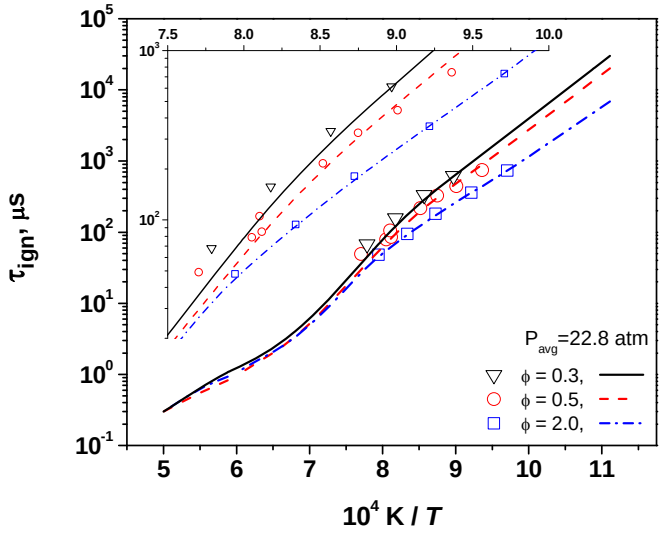

Figure 4. Ignition delay time data and modeling for P_{avg} = 22.8 atm showing equivalence ratio dependence at ϕ=0.3, 0.5, and 2.0. Symbols are experimental data, lines are current model simulations.

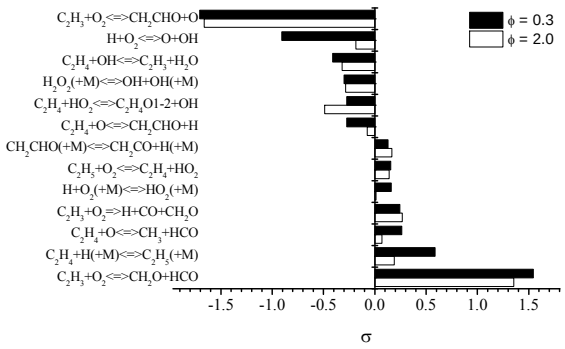

(a) T = 1000 K

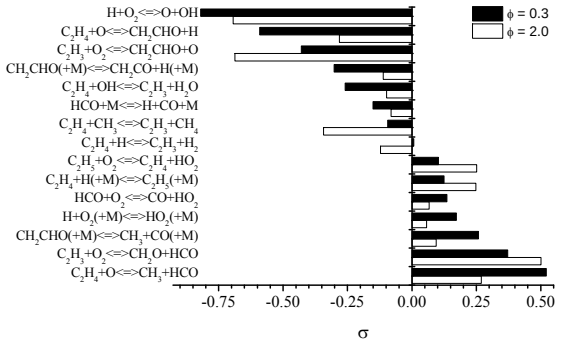

(b) T = 1200 K

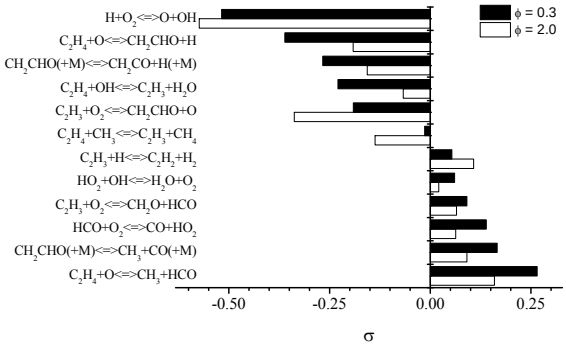

(c) T = 1400 K

Figure 5. Sensitivity analysis results performed at 1.0 atm as a function of temperature at lean and rich conditions.

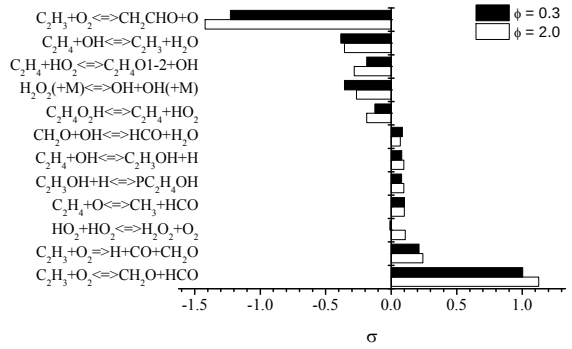

(a) T = 1000 K

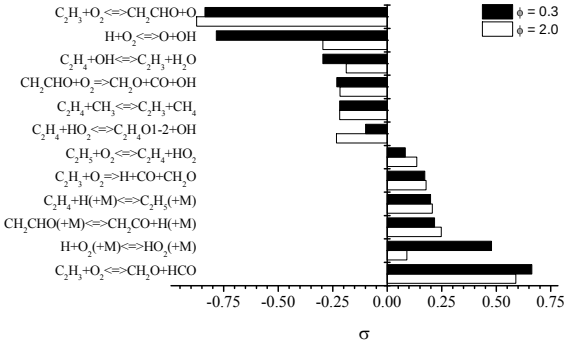

(b) T = 1200 K

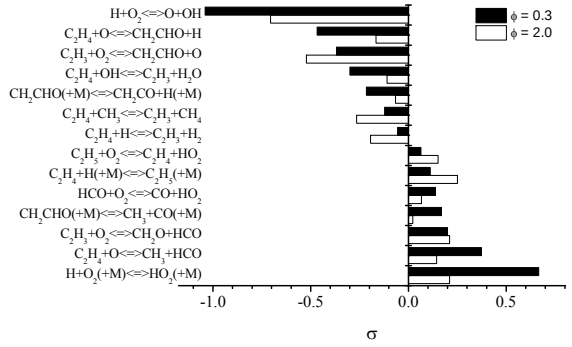

(c) T = 1400 K

Figure 6. Sensitivity analysis results performed at 22.0 atm as a function of temperature at lean and rich conditions.

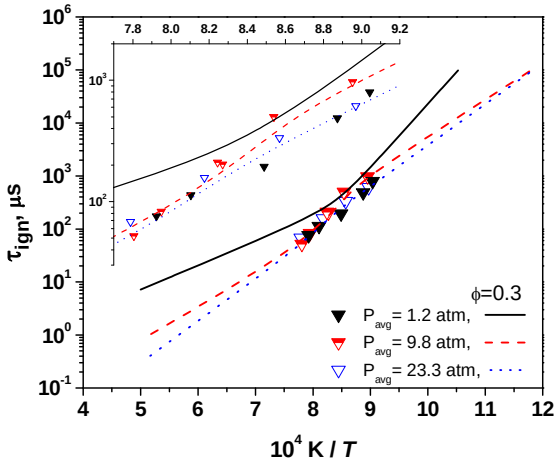

Figure 7. Ignition delay time data and modeling for ϕ = 0.3 showing pressure dependence at 1.2 atm, 9.8 atm, and 23.3 atm. Symbols are experimental data, and lines are current model simulations.

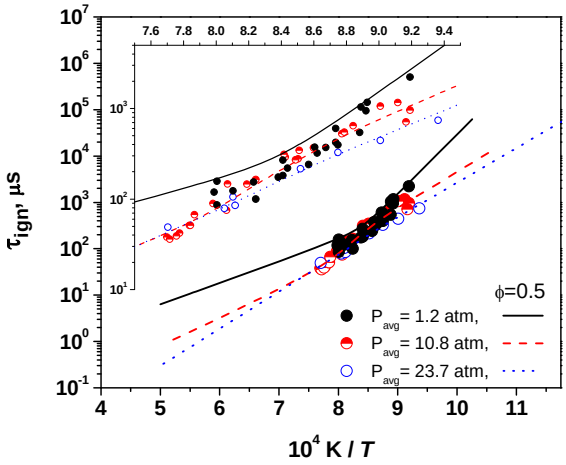

Figure 8. Ignition delay time data and modeling for ϕ = 0.5 showing pressure dependence at 1.2 atm, 10.8 atm, and 23.7 atm. Symbols are experimental data, and lines are current model simulations.

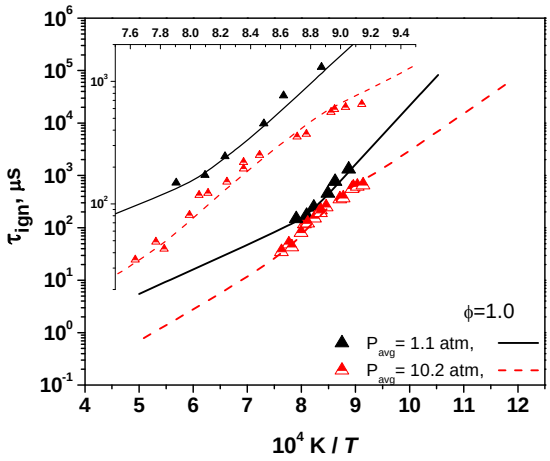

Figure 9. Ignition delay time data and modeling for ϕ = 1 showing pressure dependence at 1.1 atm and 10.2 atm. Symbols are experimental data, and lines are current model simulations.

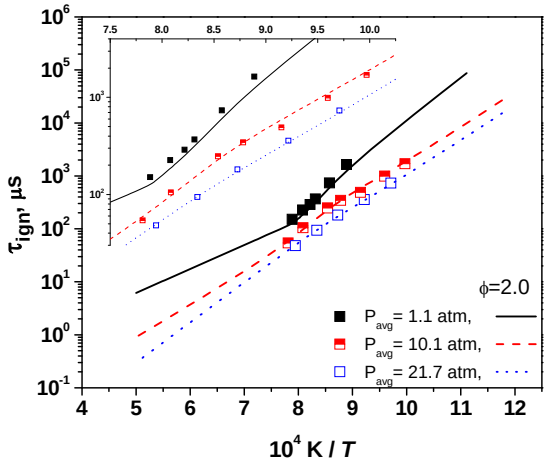

Figure 10. Ignition delay time data and modeling for ϕ = 2 showing pressure dependence at 1.1 atm, 10.1 atm, and 21.7 atm. Symbols are experimental data, and lines are current model simulations.

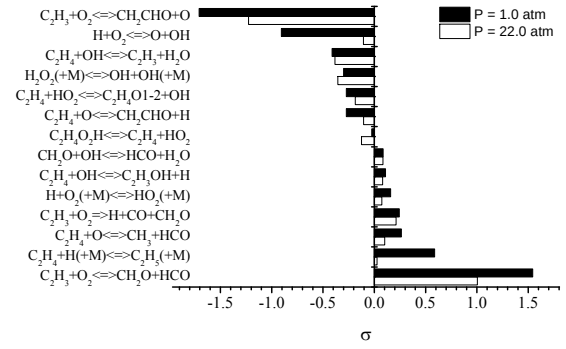

(a) 1000 K

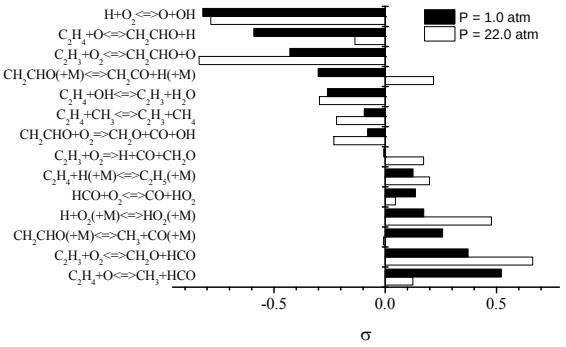

(b) 1200 K

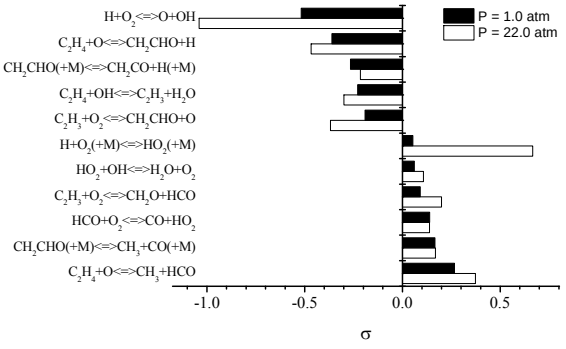

(c) 1400 K

Figure 11. Sensitivity analysis results performed at lean conditions (ϕ = 0.3) as a function of temperature at high and low pressure.

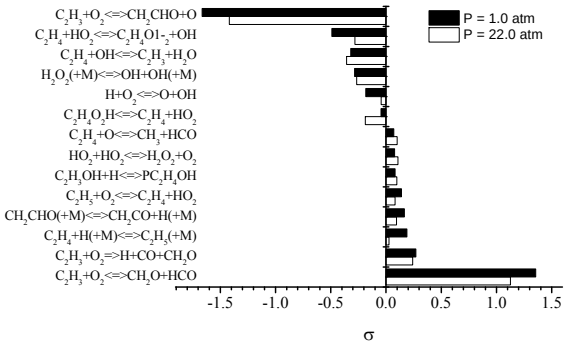

(a) 1000 K

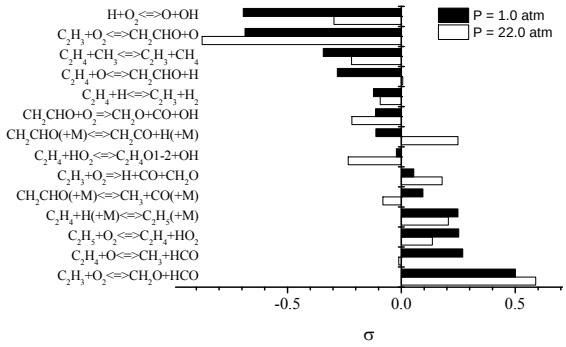

(b) 1200 K

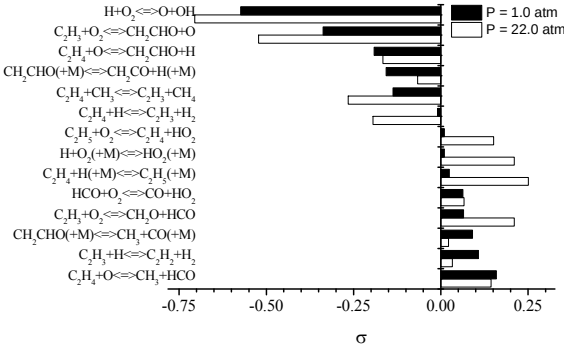

(c) 1400 K

Figure 12. **Sensitivity analysis results performed at rich conditions (ϕ = 2) as a function of temperature at high and low pressure.**

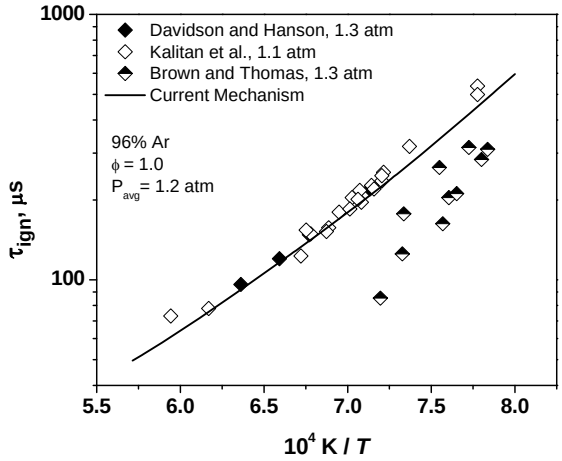

Figure 13. Comparison of dilute ignition delay time data from Davidson and Hanson [35], Kalitan *et al.* [36], and Brown and Thomas [37] for P_{avg} = 1.2 atm. Symbols are experimental data, and lines are current model simulations.

Deleted: Kalitan *et al.* [35],

Deleted: 4

Deleted: 6

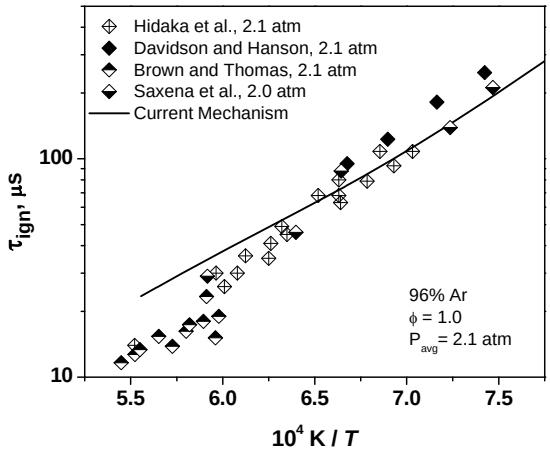

Figure 14. Comparison of dilute ignition delay time data from Davidson and Hanson [35], Brown and Thomas [37], Hidaka *et al.* [38], and Saxena *et al.* [39] for P_{avg} = 2.1 atm. Symbols are experimental data, and lines are current model simulations.

Deleted: Hidaka *et al.* [37],

Deleted: 4

Deleted: 6

Deleted: 8

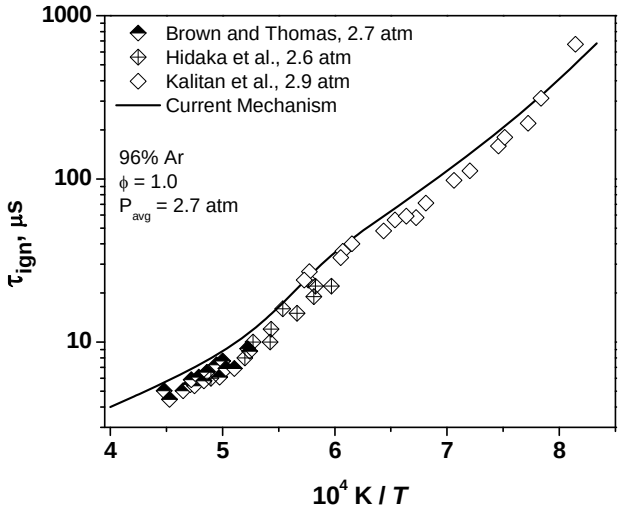

Figure 15. Comparison of dilute ignition delay time data from Kalitan *et al.* [36], Brown and Thomas [37], and Hidaka *et al.* [38], for P_{avg} = 2.7 atm. Symbols are experimental data, and lines are current model simulations.

Deleted: 5

Deleted: 7

Deleted: and Brown and Thomas [36]

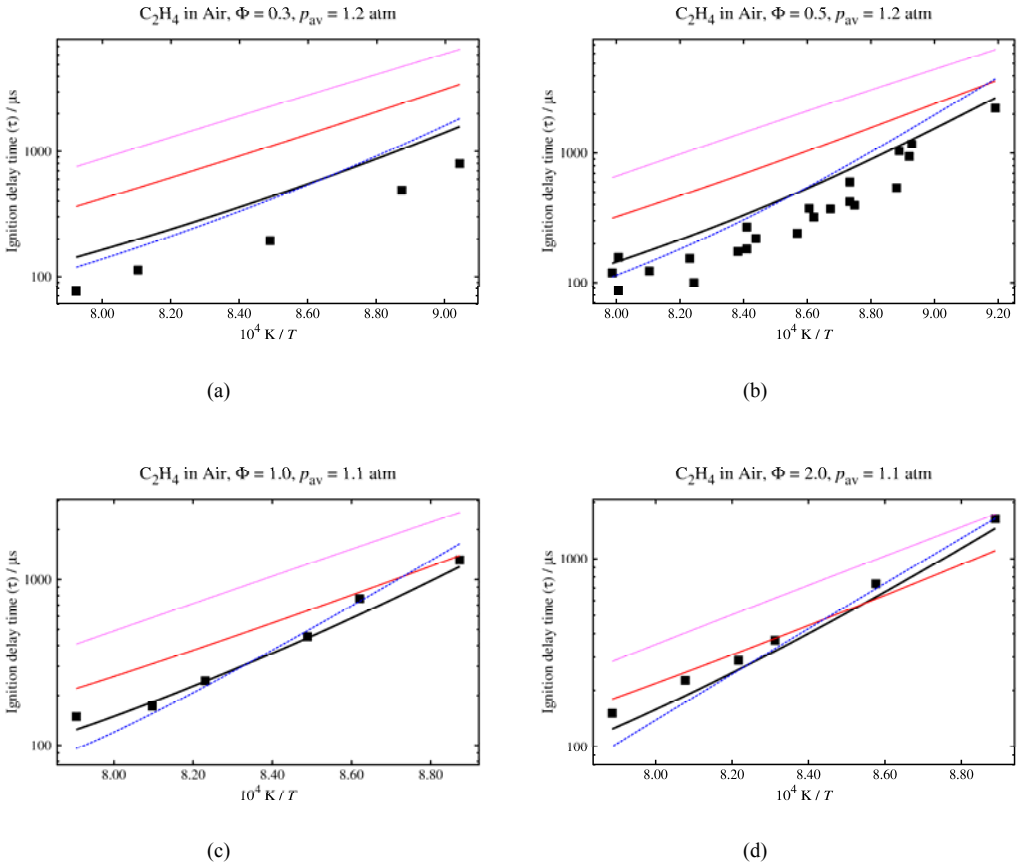

Figure 16. Predictions of various chemical kinetics models for the present data at a pressure near 1 atm. a) ϕ = 0.3, 1.2 atm; b) ϕ = 0.5, 1.2 atm; c) ϕ = 1.0, 1.1 atm; d) ϕ = 2.0, 1.1 atm. Lines are model predictions. —— current mechanism, —— a previous version of the mechanism (C4_49.0), - - - San Diego mechanism and ···· USC 2.0.

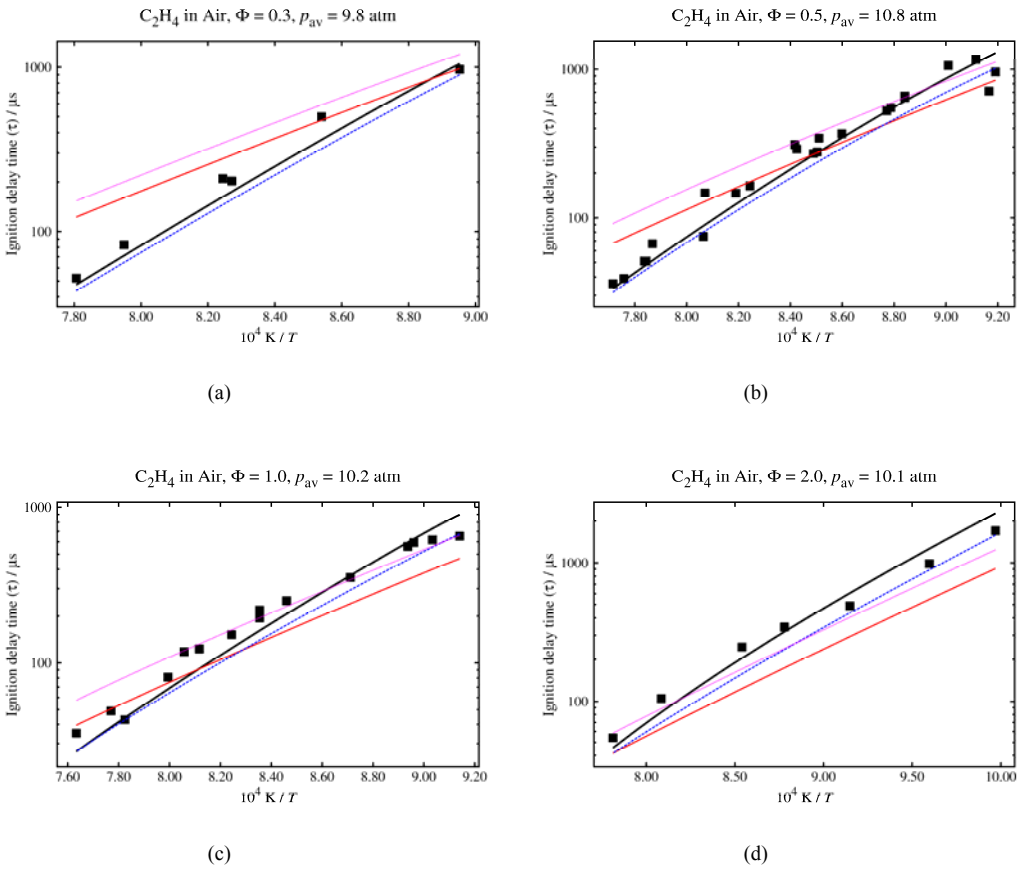

Figure 17. Predictions of various chemical kinetics models for the present data at a pressure near 10 atm. a) ϕ = 0.3, 9.8 atm; b) ϕ = 0.5, 10.8 atm; c) ϕ = 1.0, 10.2 atm; d) ϕ = 2.0, 10.1 atm. Lines are model predictions. ── current mechanism, ── a previous version of the mechanism (C4_49.0), - - - San Diego mechanism and ···· USC 2.0.

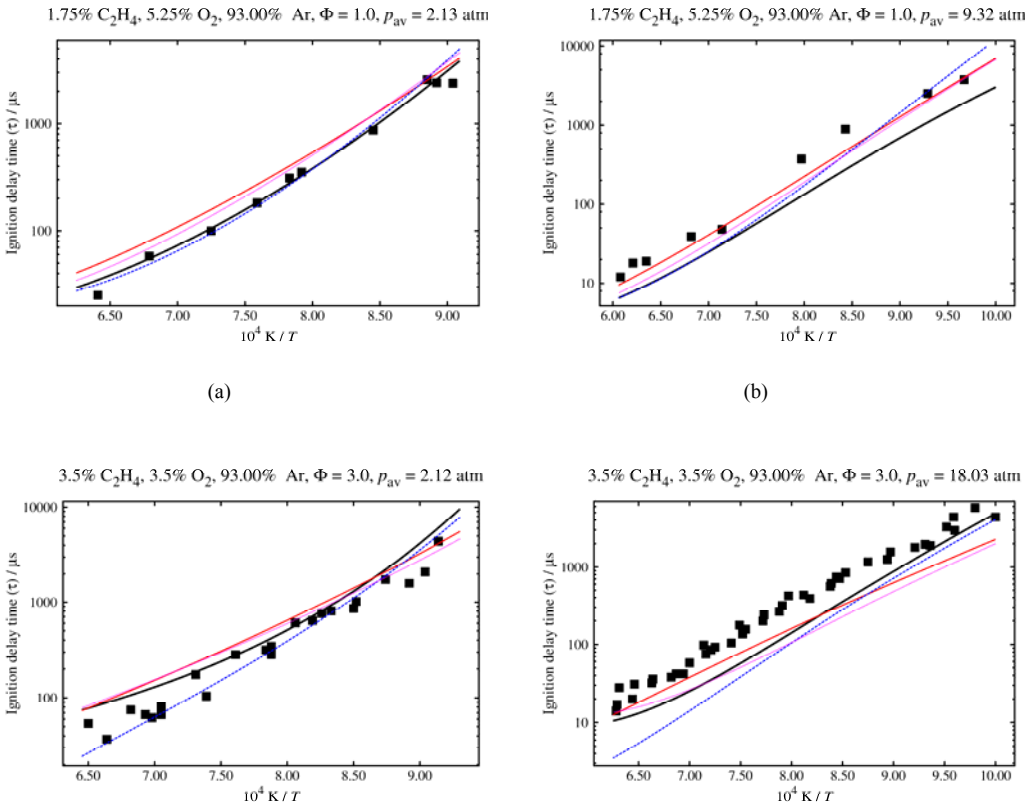

Figure 18. Predictions of various chemical kinetics models for the C_2H_4/O_2/Ar ignition delay time data of Saxena et al. [39], for 93% Argon by volume. a) ϕ = 1.0, 2.13 atm; b) ϕ = 1.0, 9.32 atm; c) ϕ = 3.0, 2.12 atm; d) ϕ = 3.0, 18.03 atm. . Lines are model predictions. — current mechanism, — a previous version of the mechanism (C4_49.0), - - - San Diego mechanism and ···· USC 2.0.

Deleted: 8

Deleted: .¶
Page Break
s

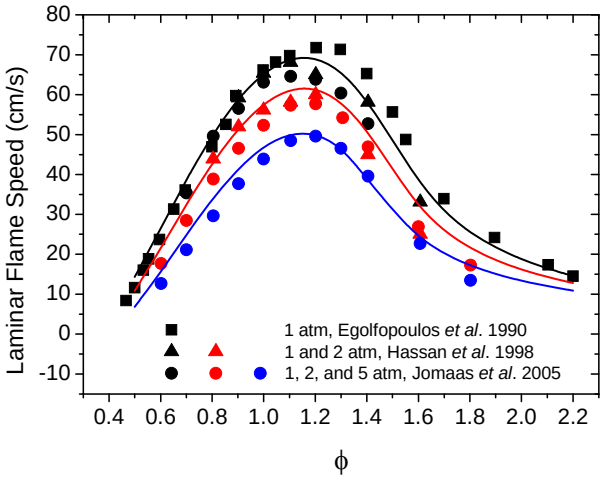

Figure 19. Laminar flame speed calculations for C_2H_4-Air mixtures for the present model (lines) compared to data from the literature. The flame speed is relative to the unburned gas. The data are from Egolfopoulos *et al.* [40], Hassan *et al.* [41], and Jomaas *et al.* [42].

Deleted: 39

Deleted: 0

Deleted: 1

Page 25: [1] Deleted	**Information Solutions & Services**	**23/09/2013 10:14:00**

C

Page 25: [1] Deleted	**Information Solutions & Services**	**23/09/2013 10:14:00**

H

Page 25: [2] Deleted	**Information Solutions & Services**	**23/09/2013 10:14:00**

H

Page 25: [2] Deleted	**Information Solutions & Services**	**23/09/2013 10:14:00**

C

Page 25: [3] Deleted	**Information Solutions & Services**	**23/09/2013 10:17:00**

O

Page 25: [3] Deleted	**Information Solutions & Services**	**23/09/2013 10:14:00**

C

Page 25: [3] Deleted	**Information Solutions & Services**	**23/09/2013 10:16:00**

C

Page 25: [4] Deleted	**Information Solutions & Services**	**23/09/2013 10:17:00**

O

Page 25: [4] Deleted	**Information Solutions & Services**	**23/09/2013 10:17:00**

C

Page 25: [4] Deleted	**Information Solutions & Services**	**23/09/2013 10:17:00**

H

Page 25: [5] Deleted	**Information Solutions & Services**	**23/09/2013 10:17:00**

O

Page 25: [5] Deleted	**Information Solutions & Services**	**23/09/2013 10:14:00**

C

Page 25: [6] Deleted	**Information Solutions & Services**	**23/09/2013 10:18:00**

O

Page 25: [6] Deleted	**Information Solutions & Services**	**23/09/2013 10:18:00**

C

Page 25: [7] Deleted	**Information Solutions & Services**	**23/09/2013 10:18:00**

O

Page 25: [7] Deleted	**Information Solutions & Services**	**23/09/2013 10:18:00**

H

Page 25: [8] Deleted	**Information Solutions & Services**	**23/09/2013 10:18:00**

O

Page 25: [8] Deleted	**Information Solutions & Services**	**23/09/2013 10:18:00**

H

Page 25: [9] Deleted	**Information Solutions & Services**	**23/09/2013 10:18:00**

O

Page 25: [9] Deleted	**Information Solutions & Services**	**23/09/2013 10:14:00**

C

Page 25: [10] Deleted	**Information Solutions & Services**	**23/09/2013 10:18:00**

C

Page 25: [10] Deleted	**Information Solutions & Services**	**23/09/2013 10:14:00**

C

Page 25: [11] Deleted	**Information Solutions & Services**	**23/09/2013 10:14:00**

C

Page 25: [11] Deleted	**Information Solutions & Services**	**23/09/2013 10:18:00**

O

Page 25: [12] Deleted	**Information Solutions & Services**	**23/09/2013 10:18:00**

O

Page 25: [12] Deleted	**Information Solutions & Services**	**23/09/2013 10:15:00**

C

Page 25: [13] Deleted	**Information Solutions & Services**	**23/09/2013 10:18:00**

O

Page 25: [13] Deleted	**Information Solutions & Services**	**23/09/2013 10:15:00**

C

Page 25: [14] Deleted	**Information Solutions & Services**	**23/09/2013 10:18:00**

O

Page 25: [14] Deleted	**Information Solutions & Services**	**23/09/2013 10:15:00**

C

Page 25: [15] Deleted	**Information Solutions & Services**	**23/09/2013 10:18:00**

O

Page 25: [15] Deleted	**Information Solutions & Services**	**23/09/2013 10:15:00**

C

Page 25: [16] Deleted	**Information Solutions & Services**	**23/09/2013 10:15:00**

C

Page 25: [16] Deleted	**Information Solutions & Services**	**23/09/2013 10:16:00**

H

Page 25: [17] Deleted	**Information Solutions & Services**	**23/09/2013 10:17:00**

C

Page 25: [17] Deleted	**Information Solutions & Services**	**23/09/2013 10:17:00**

C

Page 25: [17] Deleted	**Information Solutions & Services**	**23/09/2013 10:16:00**

H

Page 25: [18] Deleted	**Information Solutions & Services**	**23/09/2013 10:15:00**

C

Page 25: [18] Deleted	**Information Solutions & Services**	**23/09/2013 10:15:00**

C

Page 25: [18] Deleted	**Information Solutions & Services**	**23/09/2013 10:17:00**

O

Page 25: [19] Deleted	**Information Solutions & Services**	**23/09/2013 10:15:00**

C

Page 25: [19] Deleted	**Information Solutions & Services**	**23/09/2013 10:16:00**

H

Page 25: [20] Deleted	**Information Solutions & Services**	**23/09/2013 10:15:00**

C

Page 25: [20] Deleted	**Information Solutions & Services**	**23/09/2013 10:15:00**

C

Page 25: [21] Deleted	**Information Solutions & Services**	**23/09/2013 10:15:00**

C

Page 25: [21] Deleted	**Information Solutions & Services**	**23/09/2013 10:16:00**

H

Page 25: [22] Deleted	**Information Solutions & Services**	**23/09/2013 10:15:00**

C

Page 25: [22] Deleted	**Information Solutions & Services**	**23/09/2013 10:16:00**

H

Page 25: [23] Deleted	**Information Solutions & Services**	**23/09/2013 10:15:00**

C

Page 25: [23] Deleted	**Information Solutions & Services**	**23/09/2013 10:19:00**

O

Page 27: [24] Deleted	**Information Solutions & Services**	**23/09/2013 10:10:00**

O

Page 27: [24] Deleted	**Information Solutions & Services**	**23/09/2013 10:10:00**

C

Page 27: [25] Deleted	**Information Solutions & Services**	**23/09/2013 10:10:00**

H

Page 27: [25] Deleted	**Information Solutions & Services**	**23/09/2013 10:10:00**

C

Page 27: [26] Deleted	**Information Solutions & Services**	**23/09/2013 10:10:00**

O

Page 27: [26] Deleted	**Information Solutions & Services**	**23/09/2013 10:10:00**

C

Page 27: [26] Deleted	**Information Solutions & Services**	**23/09/2013 10:10:00**

C

Page 27: [27] Deleted	**Information Solutions & Services**	**23/09/2013 10:10:00**

O

Page 27: [27] Deleted	**Information Solutions & Services**	**23/09/2013 10:10:00**

C

Page 27: [27] Deleted	**Information Solutions & Services**	**23/09/2013 10:10:00**

H

Page 27: [28] Deleted	**Information Solutions & Services**	**23/09/2013 10:11:00**

C

Page 27: [28] Deleted	**Information Solutions & Services**	**23/09/2013 10:11:00**

C

Page 27: [29] Deleted	**Information Solutions & Services**	**23/09/2013 10:11:00**

H

Page 27: [29] Deleted	**Information Solutions & Services**	**23/09/2013 10:11:00**

C

Page 27: [30] Deleted	**Information Solutions & Services**	**23/09/2013 10:11:00**

C

Page 27: [30] Deleted	**Information Solutions & Services**	**23/09/2013 10:11:00**

O

Page 27: [31] Deleted	**Information Solutions & Services**	**23/09/2013 10:11:00**

C

Page 27: [31] Deleted	**Information Solutions & Services**	**23/09/2013 10:11:00**

C

Page 27: [32] Deleted	**Information Solutions & Services**	**23/09/2013 10:11:00**

C

Page 27: [32] Deleted	**Information Solutions & Services**	**23/09/2013 10:11:00**

H

Page 27: [33] Deleted	**Information Solutions & Services**	**23/09/2013 10:11:00**

C

Page 27: [33] Deleted	**Information Solutions & Services**	**23/09/2013 10:13:00**

O

Page 27: [34] Deleted	**Information Solutions & Services**	**23/09/2013 10:11:00**

C

Page 27: [34] Deleted	**Information Solutions & Services**	**23/09/2013 10:13:00**

O

Page 27: [34] Deleted	**Information Solutions & Services**	**23/09/2013 10:13:00**

O

Page 27: [35] Deleted	**Information Solutions & Services**	**23/09/2013 10:12:00**

C

Page 27: [35] Deleted	**Information Solutions & Services**	**23/09/2013 10:12:00**

H

Page 27: [35] Deleted	**Information Solutions & Services**	**23/09/2013 10:13:00**

C

Page 27: [36] Deleted	**Information Solutions & Services**	**23/09/2013 10:12:00**

C

Page 27: [36] Deleted	**Information Solutions & Services**	**23/09/2013 10:12:00**

C

Page 27: [37] Deleted	**Information Solutions & Services**	**23/09/2013 10:12:00**

H

Page 27: [37] Deleted	**Information Solutions & Services**	**23/09/2013 10:13:00**

O

Page 27: [37] Deleted	**Information Solutions & Services**	**23/09/2013 10:13:00**

O

Page 27: [38] Deleted	**Information Solutions & Services**	**23/09/2013 10:12:00**

H

Page 27: [38] Deleted	**Information Solutions & Services**	**23/09/2013 10:12:00**

C

Page 27: [39] Deleted	**Information Solutions & Services**	**23/09/2013 10:12:00**

H

Page 27: [39] Deleted	**Information Solutions & Services**	**23/09/2013 10:13:00**

O

Page 27: [40] Deleted	**Information Solutions & Services**	**23/09/2013 10:12:00**

H

Page 27: [40] Deleted	**Information Solutions & Services**	**23/09/2013 10:13:00**

O

Page 27: [41] Deleted	**Information Solutions & Services**	**23/09/2013 10:12:00**

H

Page 27: [41] Deleted	**Information Solutions & Services**	**23/09/2013 10:12:00**

C

Page 27: [42] Deleted	**Information Solutions & Services**	**23/09/2013 10:12:00**

H

Page 27: [42] Deleted	**Information Solutions & Services**	**23/09/2013 10:13:00**

C